MBOAT7 and CDS2 coordinate lipid droplet dynamics and cholesterol metabolism in liver

Jiesi Xu[1, 2, *], Jianxin Zhang[2, 3, *], Wei Wang[2], Honggang Su[2, 3], Siyu Chen[4], Mei Ding[2,] and Xun Huang[2, 5, #]

1. The Key Laboratory of Geriatrics, Beijing Institute of Geriatrics, Institute of Geriatric Medicine, Chinese Academy of Medical Sciences, Beijing Hospital/National Center of Gerontology of National Health Commission, Beijing, 100730, China

2. Institute of Genetics and Developmental Biology, Chinese Academy of Sciences, Beijing 100101, China

3. University of Chinese Academy of Sciences, Beijing 100049, China

4. Medical Research Center, Beijing Institute of Respiratory Medicine and Beijing Chao-Yang Hospital, Capital Medical University, Beijing 100020, China

5. Tianjian Laboratory of Advanced Biomedical Sciences, Zhengzhou University, Zhengzhou 450001, China

* Equal contribution

To whom correspondence should be addressed at: Institute of Genetics and Developmental Biology, Chinese Academy of Sciences, Beijing 100101, China

86-10-64806560 (Tel & Fax)

Email: xhuang@genetics.ac.cn

Abstract

Metabolic dysfunction-associated steatotic liver disease (MASLD) affects 20%–25% of the global population. A common genetic variant, rs641738, in the membrane-bound O-acyltransferase 7 (MBOAT7) gene, is strongly associated with disease progression. However, the physiological function and regulatory mechanisms of MBOAT7 remain incompletely understood. Lipid droplet (LD) accumulation is a hallmark of MASLD. In this study, we reveal a coordinated role of MBOAT7 and CDP-diacylglycerol synthase 2 (CDS2) in regulating LD size and cholesterol metabolism. Under normal conditions, CDS2 interacts with MBOAT7 at the endoplasmic reticulum (ER). In the absence of CDS2, however, MBOAT7 relocates to ER-LD contact sites in a RAB1-dependent manner, where it competes with DGAT2 for RAB1 binding. This competition inhibits LD expansion and promotes lipolysis. This MBOAT7-mediated LD size reduction activates the AMPK-LXR axis, enhancing cholesterol excretion, while loss of MBOAT7 or CDS2 disrupts this pathway, leading to hepatic cholesterol accumulation. Together, our study identifies a CDS2-MBOAT7-RAB1 regulatory axis controlling LD homeostasis and cholesterol metabolism.

Introduction

Metabolic dysfunction-associated steatotic liver disease (MASLD) is the most common chronic liver disorder worldwide, affecting 20%-25% of the general population [1,2]. Inadequate understanding of the underlying mechanism has hindered the development of drugs to treat the disease. Genetic predisposition is clearly an important factor in the pathogenesis of the disease [3].

The MBOAT7 (membrane-bound O-acyltransferase 7) variant rs641738 (C>T, loss of function mutation) has been strongly linked to all stages of MASLD, including steatosis, inflammation and fibrosis [4-7]. MBOAT7 exhibits lysophosphatidylinositol (LPI) acyltransferase activity, preferentially incorporating arachidonic acid into phosphatidylinositol (PI) as part of the PI remodeling pathway, also known as the Lands' cycle [8]. PI can also be synthesized *de novo* via the Kennedy pathway. A key step in this pathway is the formation of CDP-diacylglycerol (CDP-DAG) in liver, catalyzed by CDS (CDP-DAG synthase) [8,9]. Notably, CDS2 is selectively inhibited by PI species containing arachidonoyl chains (PI-AA), indicating a potential link between MBOAT7 and CDS2 [10]. Previous studies have shown that *Mboat7* depletion leads to lipid accumulation and metabolic dysfunction-associated steatohepatitis (MASH), partly through increasing CDS2 activity [11,12]. However, our earlier work demonstrated that deletion of *Cds2* in mice leads to spontaneous development of MASH, phenocopying the effects of MBOAT7 loss-of-function [13]. CDS2 deficient mammalian cells have elevated lipid accumulations [14,15]. These findings highlight a complex regulatory interplay between MBOAT7 and CDS2 in lipid metabolism, underscoring the need for further investigation into their roles in MASLD.

Lipid droplets (LD) accumulation is a defining characteristic of MASLD [16]. The surface of LDs hosts specific proteins, some of which are also ER proteins [17,18]. Proteins can target the LD monolayer from the ER bilayer, either during LD formation or later via ER-LD bridges [19]. This ER-to-LD targeting process requires membrane-fusion proteins such as Rabs, membrane-tethering complex components, and SNAREs [20-22]. MBOAT7 has been identified in the ER, ER-associated membranes (MAMs), and LD fractions [23,24], however, the mechanism by which MBOAT7 targets

LDs and its precise role on LDs remain poorly understood. CDS2 is enriched in ER and MAMs [13]. Depletion of CDS2 results in the formation of "supersized" LDs [14,15].

Here, we report that MBOAT7 and CDS2 jointly regulate LD size and cholesterol metabolism. Mechanistically, MBOAT7 is primarily localized to the ER, but in CDS2-deficient cells, MBOAT7 relocates to ER-LD contacts with the help of RAB1. Our findings show that CDS2 depletion increases LD size, while expression of MBOAT7 reduces LD size in CDS2-deficient cells. Moreover, LD-associated MBOAT7 promotes lipolysis and inhibits the targeting of DGAT2 to LDs, activating the AMPK-LXR axis and enhancing cholesterol excretion. Conversely, knockdown of either *Mboat7* or *Cds2* suppresses the AMPK-LXR axis, leading to increased cholesterol content in liver. This study demonstrates that MBOAT7 and CDS2 regulate LD dynamics and cholesterol metabolism, revealing their roles in the pathogenesis of MASLD.

Results

MBOAT7 and CDS2 regulate cholesterol and fatty acid metabolism in liver

To investigate the connection between MBOAT7 and CDS2, we analyzed hepatic transcriptome datasets and GEPIA (Gene Expression Profiling Interactive Analysis). This showed that *MBOAT7* and *CDS2* expression levels in human liver samples are positively correlated (Figure 1A-C). Both *MBOAT7* and *CDS2* are upregulated in liver tumor samples compared with non-tumor liver samples (Figure S1A). To determine the roles of MBOAT7 and CDS2 in the regulation of hepatic lipid metabolism, we specifically knocked down these enzymes in the liver by injecting C57BL/6 mice with AAV-TBG-sh*Mboat7*, AAV-TBG-sh*Cds2* or AAV-TBG-sh*Mboat7*+AAV-TBG-sh*Cds2* (Figure 1D). Consistent with previous report [25], knockdown of *Mboat7* in liver did not affect plasma lipid content but increased hepatic triglyceride and cholesterol content (Figure 1E-F and Figure S1B-C). Knockdown of *Cds2* did not affect plasma triglyceride content, but increased plasma and hepatic cholesterol and hepatic triglyceride content (Figure 1E-F and Figure S1B-C). Knockdown of both *Mboat7* and *Cds2* did not further enhance triglyceride

and cholesterol content (Figure 1E-F and Figure S1B-C), indicating that combined knockdown of *Mboat7* and *Cds2* did not exert additive effects on the increased lipid levels. Consistent with the above results, H&E staining showed that knockdown of *Mboat7*, *Cds2*, and *Mboat7* + *Cds2* increased hepatic steatosis (Figure 1G-H).

To examine the pathways regulated by MBOAT7 and CDS2, we performed RNA sequencing (RNAseq) analysis on liver from the sh*Mboat7*, sh*Cds2*, and sh*Mboat7* + sh*Cds2* groups. When we compared the results, we noticed an extensive overlap between the three datasets: 266 genes were significantly upregulated and 301 genes were significantly downregulated in all three groups (Figure 1I). Kyoto Encyclopedia of Genes and Genomes (KEGG) analysis revealed significant changes in cholesterol and fatty acid metabolism pathways among the genes with downregulated expression in all three groups (Figure 1J). For the genes with upregulated expression in all three groups, KEGG analysis revealed significant alterations in steroid biosynthesis and non-alcoholic fatty liver pathways (Figure S1D). LXR, a key regulator of cholesterol efflux, controls the transcription levels of genes such as *Abca1* and *Abcg5/8*. Our qPCR analysis showed that genes involved in cholesterol excretion (*Lxr*, *Abcg8* and *Abca1*) were downregulated in liver (Figure 1K), indicating that reduced expression of *Mboat7* or *Cds2* impairs cholesterol excretion. Knockdown of *Mboat7* and *Cds2* increased the expression of *Fasn*, which regulates fatty acid biosynthesis (Figure 1K). Accordingly, LXR protein levels were reduced in the liver of sh*Mboat7*, sh*Cds2*, and sh*Mboat7*+sh*Cds2* mice (Figure 1L and Figure S1E). Nuclear SREBP2 and HMGCR levels were diminished, likely due to feedback inhibition of cholesterol biosynthesis by increased cellular cholesterol levels (Figure 1L and Figure S1E). ALT and AST measurements revealed that knockdown of *Mboat7* or *Cds2* or both did not exacerbate liver inflammation (Figure S1F and G). Overall, these data suggests that MBOAT7 and CDS2 coordinate fatty acid and cholesterol metabolism.

MBOAT7 is localized to the ER-LD contacts in lipid-loaded CDS2 KO cells

To investigate how MBOAT7 and CDS2 cooperatively regulate lipid metabolism, we focused on lipid droplets (LDs). Previous studies have shown that CDS2 knockout

increases LD size [15]. We examined the localization and roles of MBOAT7 in LD regulation. MBOAT7-EGFP exhibited an ER-like localization pattern in both wild-type and CDS2 KO HeLa cells (Figure S2A and B). Interestingly, in CDS2 KO cells treated with oleic acid (OA) to induce LD formation, MBOAT7-EGFP (Figure 2A-B) and MBOAT7-mCherry (Figure S2C-D) surrounded LDs stained by LipidTOX and BODIPY, respectively. In contrast, MBOAT7-EGFP did not show colocalization with LDs in OA-treated control HeLa cells (Figure 2A-B). Furthermore, in OA-treated CDS2 KO cells, MBOAT7-EGFP was colocalized with the LD marker mScarlet-PLIN1, whereas no such colocalization was observed in control cells (Figure S2E). Similarly, in OA-treated HepG2 cells, MBOAT7-EGFP remained localized to the ER, but enclosed LDs when CDS2 was knocked down (Figure S2F). We also analyzed the localization of endogenous MBOAT7. In OA-treated CDS2 KO cells, endogenous MBOAT7 colocalized with LDs, but this was not observed in OA-treated control cells (Figure 2C-D). 3D reconstruction of the LD surface confirmed that MBOAT7 localized to the LD surface in OA-treated CDS2 KO cells (Figure 2E).

The colocalization of MBOAT7 with LDs in CDS2 KO cells led us to test whether CDS2 depletion affects the targeting of other ER proteins to LDs. The ER marker mScarlet-SEC61b did not colocalize with LDs in OA-loaded CDS2 KO cells (Figure 2F-G). Since CDS2 protein levels are downregulated in MASLD mouse models [13], we also tested whether MBOAT7 targets to LDs in the liver of MASLD model mice, in which MASLD is induced by the feeding with the fat/fructose/cholesterol-rich Gubra-Amylin NASH (GAN) diet. Confocal imaging showed that endogenous MBOAT7 was more enriched at the LD periphery in liver sections from GAN diet-induced MASLD mice compared to those from normal mice (Figure 2H-I). Since MBOAT7 is a multipass transmembrane protein, it is likely localized to the ER regions adjacent to LDs, rather than to the LD membrane. These findings suggest that MBOAT7 specifically localizes to the ER-LD contacts in lipid-overloaded CDS2-deficient cells but not in control cells.

The N-terminus of MBOAT7 is required for localization of MBOAT7 to ER-LD contacts in CDS2 KO cells

MBOAT7 consists of 11 transmembrane (TM) helices organized into two bundles (TM1-5 and TM9-11) that tilt apart, creating a central catalytic chamber [26] (Figure 3A). To identify the region required for the localization of MBOAT7 to ER-LD contacts, we generated three EGFP-tagged truncated versions of MBOAT7, containing the N-terminal region (amino acids 1-135), the central region (180-310), and the C-terminal region (311-472) (Figure 3A). Only the N-terminal region localized to ER-LD contacts in CDS2 KO cells, and MBOAT7 with a deletion of the N-terminal 99 amino acids did not localize to ER-LD contacts (Figure 3B). We further investigated the specific TM regions critical for LD targeting in CDS2 KO cells. Deleting TM1-2 slightly disrupted MBOAT7's ring-like pattern on LDs, while deleting TM3-4 completely abolished its LD anchoring (Figure 3C). To validate the importance of TM3-4 for ER-LD localization, we generated chimeric proteins by swapping TM3 or TM4 with the corresponding regions from MBOAT5, which belongs to the membrane-bound O-acyltransferase (MBOAT) family and carries out re-acylation of phosphatidylserine (PS) and phosphatidylcholine (PC) on ER. MBOAT7 and MBOAT5 have similar structure [26]. These chimeric proteins failed to localize to LDs (Figure 3D). Therefore, the N-terminus of MBOAT7, particularly TM3-4, is required for the localization of MBOAT7 to ER-LD contacts in CDS2 KO cells.

MBOAT7 interacts with CDS2

Next, we examined why MBOAT7 is localized to the ER-LD contacts in CDS2 KO cells but not in control cells. Similar to MBOAT7, CDS2 is localized to the ER and MAMs [13]. We hypothesized that CDS2 retains MBOAT7 at the ER, while MBOAT7 relocates to the ER-LD contacts in the absence of CDS2. Co-immunoprecipitation (co-IP) assays demonstrated that Flag-CDS2 precipitated MBOAT7-EGFP (Figure 3E), and conversely, MBOAT7-EGFP precipitated Flag-CDS2 (Figure 3F). Using CRISPR-based knock-in (KI) of EGFP at the N-terminus of endogenous CDS2, we

found that endogenous CDS2 coprecipitated with endogenous MBOAT7 (Figure 3G). To examine the direct binding between these two proteins, we purified His-MBOAT7 from *E. coli* and Flag-CDS2 from mammalian cells. Western blot analysis confirmed their direct interaction (Figure 3H). Overall, these results indicate that CDS2 interacts with MBOAT7, retaining it at the ER.

RAB1 is required for localization of MBOAT7 at ER-LD contacts in CDS2 KO cells

Next, we investigated how MBOAT7 targets to the ER-LD contacts in CDS2 KO cells. ER proteins typically target the LD monolayer surface, which requires membrane continuity between the ER outer leaflet and the LD monolayer [19]. This targeting can occur either during early LD formation or to mature LDs after their formation. These ER proteins associate with the LD monolayer through hydrophobic hairpins, which insert midway into the lipid bilayers of the ER, with both the N- and C-termini facing the cytosol [27]. MBOAT7, however, is a multispanning transmembrane protein with 11 transmembrane domains, making it unlikely that MBOAT7 localizes directly to the LD monolayer. Since MBOAT7 lacks a hairpin structure, we hypothesized that ER-localized MBOAT7 associates with LDs in CDS2 KO cells via interaction with LD-associated proteins.

We immunoprecipitated MBOAT7-EGFP from control and CDS2 KO cells and identified its interacting proteins using LC-MS/MS (Figure 4A). We hypothesized that MBOAT7 would interact with LD proteins in CDS2 KO cells but not in control cells, so we selected candidates whose interaction with MBOAT7 in CDS2 KO cells was at least 2-fold stronger than in control cells. Based on previously published LD proteomes [28-30], we focused on LD proteins. Five proteins from our dataset were shared with all the published LD proteomes (Figure 4B). Interestingly, of these five candidates, four of them are RAB proteins (RAB1A, RAB7A, RAB14 and RAB18) (Figure 4C). RAB1 mediates targeting triglyceride biosynthetic enzymes to LDs [20,31]. Our results showed that knockdown of RAB1A impaired the LD targeting of MBOAT7 in OA-loaded CDS2 KO cells (Figure 4D-F). Co-IP assays showed that

MBOAT7-EGFP interacted with Flag-RAB1A in CDS2 KO cells but not in control cells, suggesting that RAB1A helps MBOAT7 target to the ER-LD contacts in CDS2 KO cells (Figure 4G). Furthermore, expressing HA-tagged CDS2 in CDS2 KO cells inhibited the interaction between MBOAT7 and RAB1A (Figure 4H). We then determined the binding sites between MBOAT7 and RAB1A. MBOAT7 structure were shown previously [26]. The crystal structure of RAB1A was predicted using AlphaFold3, and the 3D structure of MBOAT7/RAB1A docking was simulated. The results showed that the amino acid residues F134, S135, E178 in MBOAT7 and the amino acid residues F73, Y80, K90 in RAB1A were the potential interaction sites (Figure 4I). Mutation of the predicted binding sites within MBOAT7 to alanine abrogated their interaction (Figure 4J). Together, these results suggest that RAB1A is essential for targeting of MBOAT7 to the ER-LD contacts in CDS2 KO cells, and that CDS2 inhibits this targeting by competing with RAB1A for binding to MBOAT7.

MBOAT7 reduces LD size in CDS2 KO cells by inhibiting the targeting of DGAT2 to LDs

We next investigated the function of ER-LD contact-localized MBOAT7. Overexpression of MBOAT7-EGFP did not affect LD size in control cells, but it reduced LD size in CDS2 KO cells (Figure 5A-B). Overexpression of an MBOAT7 mutant with reduced catalytic activity (MBOAT7(N321A, H356A)-EGFP) still reduced the LD size in CDS2 KO cells (Figure 5A-B). This indicates that the effect of MBOAT7 on LD size reduction in CDS2 KO cells is independent of its enzymatic activity.

To explore the underlying mechanism, we considered previous findings suggesting that the lipid biosynthetic enzymes DGAT2 and GPAT4 target LDs earlier in CDS2 KO cells than in control cells, promoting LD growth [14]. The previous study also showed that knockdown of DGAT2 or GPAT4 reduced the LD size in CDS2 KO cells [14]. Since RAB1 is required for targeting of DGAT2 and GPAT4 to LDs [20,31], we hypothesized that MBOAT7 may impede the LD targeting of DGAT2 or GPAT4 by competitively interacting with RAB1, thus limiting LD growth in CDS2 KO cells.

Consistent with this idea, we found that both Flag-DGAT2 and Flag-GPAT4 bound to GFP-tagged RAB1A (Figure 5C and D). Importantly, MBOAT7-EGFP expression reduced the binding between Flag-DGAT2 and GFP-RAB1A in CDS2 KO cells (Figure 5E). When the interaction between MBOAT7 and RAB1A is disrupted, the binding between Flag-DGAT2 and GFP-RAB1A is retained (Figure 5E). Conversely, knockdown of MBOAT7 enhanced the binding between Flag-DGAT2 and GFP-RAB1A in CDS2 KO cells (Figure 5F). Confocal images showed that EGFP-DGAT2 was targeted to LDs in CDS2 KO cells, but overexpression of MBOAT7-mCherry blocked this targeting (Figure 5G). The interaction between GPAT4 and RAB1A was unaffected by MBOAT7 overexpression (Figure S3A). Both Flag-DGAT2 and Flag-MBOAT7 interact with full-length GFP-RAB1A; however, their interactions are markedly reduced when RAB1A is truncated at either the N-terminus or the C-terminus (Figure 5H-I). In response to OA treatment, triglyceride synthesis enzymes like DGAT2 or GPAT4 are more likely to target to LDs to promote LD growth [32]. Since this process requires RAB1, we then tested whether OA treatment affects the interaction of these enzymes with RAB1. OA treatment enhanced DGAT2 binding to RAB1A but did not affect GPAT4 binding to RAB1A (Figure 5J and Figure S3B). Interestingly, MBOAT7 binding to RAB1A increased after OA treatment in CDS2 KO cells (Figure 5K). Taken together, our data suggest that CDS2 retains MBOAT7 at the ER. When CDS2 is absent, MBOAT7 binds to RAB1 and localizes to the ER-LD contacts. Furthermore, MBOAT7 reduces the size of LDs by inhibiting the targeting of DGAT2 to LDs.

MBOAT7 regulates LD size and lipolysis in the absence of CDS2

The studies above reveal the regulatory roles of MBOAT7 and CDS2 in controlling LD size in cultured cells. We next examined how MBOAT7 and CDS2 functionally interact and regulate LD size *in vivo*. Since MBOAT7 and CDS2 are bound to each other, we tested whether CDS2 affects the acyltransferase activity of MBOAT7 using MBOAT7 substrates like lyso-PI and [14C]-arachidonic acid. We analyzed the activity of MBOAT7 in the liver from control mice (*Cds2*$^{f/f}$), mice with liver-specific

depletion of CDS2 (*Cds2*$^{f/f}$*;AlbCre*), and hepatic CDS2-depleted mice with AAV-mediated hepatic re-expression of CDS2 (*Cds2*$^{f/f}$*;AlbCre* + AAV-CDS2). The results showed that CDS2 deficiency did not significantly impact the enzymatic activity of MBOAT7 (Figure 6A).

To determine how MBOAT7 and CDS2 regulate LDs *in vivo*, *Cds2*$^{f/f}$ and *Cds2*$^{f/f}$*;AlbCre* mice were injected with AAV-TBG-Con or AAV-TBG-*Mboat7* (Figure 6B). Hepatic overexpression of *Mboat7* did not affect plasma lipids in either control or *Cds2*$^{f/f}$*;AlbCre* mice (Figure S4A-B). Hepatic overexpression of *Mboat7* did not change hepatic triglyceride and cholesterol levels in *Cds2*$^{f/f}$ mice, but it reduced hepatic cholesterol levels in *Cds2*$^{f/f}$*;AlbCre* mice (Figure 6C and D). H&E staining showed that liver sections from *Cds2*$^{f/f}$*;AlbCr*e mice contained "supersized" LDs, while overexpression of *Mboat7* reduced the LD size in *Cds2*$^{f/f}$*;AlbCre* mice, resulting in multiple small-sized LDs in hepatocytes (Figure 6E). This reduction in LD size was also confirmed in *Cds2*-deficient primary hepatocytes (Figure 6F and G). Cell fractionation assays revealed that overexpression of *Mboat7* reduced the protein level of DGAT2 in the LD fraction from the livers of *Cds2*$^{f/f}$*;AlbCre* mice, while increasing the protein level of ATGL (also called PNPLA2) (Figure 6H), a rate-limiting enzyme for lipolysis. To test if MBOAT7 regulates lipolysis, we used isoprenaline (ISO) to stimulate lipolysis. The results showed that overexpression of MBOAT7 increased free fatty acid (FFA) release in both DMSO and ISO-treated *Cds2*-deficient primary hepatocytes (Figure 6I).

Overall, our data suggest that MBOAT7 controls LD size and lipolysis by inhibiting DGAT2 targeting to LDs and promoting ATGL targeting to LDs in both CDS2-deficient cell lines and primary hepatocytes.

MBOAT7 and CDS2 regulate cholesterol metabolism through the AMPK pathway

We next investigated the physiological significance of ER-LD contact-localized MBOAT7. Our results showed that knockdown of *Mboat7* reduced the expression levels of genes in the liver X receptor (LXR) pathway, suggesting impaired

cholesterol excretion (Figure 1K-L). Heatmap analysis further confirmed the downregulation of genes involved in cholesterol excretion (Figure S4C). We then explored how cholesterol excretion is regulated by MBOAT7 and CDS2. Activation of the AMPK pathway is known to inhibit SREBP and enhance LXR protein levels [33]. Interestingly, AMPK signaling was downregulated in the liver of sh*Mboat7*, sh*Cds2*, or sh*Mboat7* + sh*Cds2* mice, as indicated by heatmap analysis and western blotting (Figure S4C-E). In contrast, overexpression of *Mboat7* increased p-AMPK and p-ACC levels in *Cds2*$^{f/f}$*;AlbCre* mice, suggesting that AMPK pathway activity was enhanced (Figure 7A-B). This was accompanied by reduced nuclear SREBP2 levels and increased expressions of LXR and its target ABCA1 in *Cds2*$^{f/f}$*;AlbCre* mice (Figure 7A-B). Accordingly, mRNA analysis revealed that downstream targets of LXR (*Abca1*, *Abcg5* and *Abcg8*) were upregulated in the liver of *Mboat7*-overexpressing *Cds2*$^{f/f}$*;AlbCre* mice (Figure 7C). To confirm whether MBOAT7 regulates cholesterol excretion via the AMPK pathway in *Cds2*$^{f/f}$*;AlbCre* mice, we treated primary hepatocytes from *Cds2*$^{f/f}$*;AlbCre* mice with Ad-EGFP and Ad-MBOAT7-EGFP and the AMPK inhibitor dorsomorphin. The results showed that dorsomorphin blocked the ability of *Mboat7* to elevate LXR protein levels (Figure 7D). This demonstrates that MBOAT7 regulates cholesterol excretion via the AMPK-LXR axis.

We then explored how overexpression of MBOAT7 increases AMPK activity in *Cds2*$^{f/f}$*;AlbCre* mice. Lipolysis regulates key intracellular nutrient-sensing pathways, such as the AMPK pathway. Genetic or pharmacological activation of lipolysis activates AMPK by elevating intracellular AMP content [34]. Since MBOAT7 overexpression promotes lipolysis in *Cds2*-deficient primary hepatocytes (Figure 6I), we examined whether this process activates AMPK in primary hepatocytes. Activation of lipolysis with isoprenaline (ISO) enhanced AMPK activity in wild-type primary hepatocytes under both Ad-EGFP and Ad-MBOAT7-EGFP conditions (Figure S4F-G). Conversely, inhibiting lipolysis with the ATGL inhibitor Atglistatin (ATGLi) reduced AMPK signaling (Figure S4H-I), which demonstrates that lipolysis regulates AMPK signaling in primary hepatocytes. In *Cds2*-deficient primary

hepatocytes, overexpression of MBOAT7 activated AMPK signaling, which was further enhanced by ISO treatment (Figure 7E-F). Importantly, ATGLi treatment diminished AMPK activation caused by MBOAT7 overexpression in *Cds2*-deficient primary hepatocytes (Figure 7G-H), demonstrating that MBOAT7 regulates AMPK activity at least partially by promoting lipolysis. These findings suggest that *Mboat7* reduces LD size and cholesterol content in *Cds2*-deficient conditions by activating the AMPK-LXR axis.

AMPK agonist ameliorates *Cds2*- or *Mboat7*-deficiency-induced MASLD

Since *Cds2* and *Mboat7* deficiency resulted in downregulation of the AMPK pathway and impaired cholesterol excretion, we investigated whether pharmacological activation of AMPK could reverse the MASLD phenotype in *Cds2*- or *Mboat7*-deficient mice. 8-week-old mice were injected with either AAV-TBG-sh*Cds2* or AAV-TBG-sh*Mboat7* and concurrently fed a NASH-inducing GAN diet for 4 weeks. During the final 2 weeks of this period, mice received intraperitoneal injections of the AMPK agonist A769662 (30 mg/kg, twice daily; Figure 8A). Following A769662 treatment, body weight was reduced in both *Cds2*- and *Mboat7*-deficient mice (Figure 8B). Although plasma triglyceride and cholesterol levels remained unchanged, hepatic levels of triglyceride and cholesterol were significantly decreased (Figure 8C-F). Additionally, A769662 treatment lowered plasma ALT levels, indicating reduced liver inflammation (Figure 8G). H&E and Oil-Red-O staining confirmed a marked reduction in hepatic lipid accumulation in A769662-treated mice compared to vehicle controls (Figure 8H). To assess downstream signaling, we examined the AMPK-LXR axis. A769662 treatment increased both mRNA and protein levels of LXR and ABCA1 in sh*Cds2* and sh*Mboat7* livers (Figure 8I-J and Figure S4J). Together, these findings suggest that AMPK activation can effectively ameliorate MASLD phenotypes caused by *Cds2* or *Mboat7* deficiency.

Discussion

Here we identified a coordinated role of MBOAT7 and CDS2 in regulating LD size. At the ER, CDS2 binds to MBOAT7, but in the absence of CDS2, MBOAT7 locates to the ER-LD contacts. This relocation promotes lipolysis and inhibits the targeting of DGAT2 to LDs in a RAB1-dependent manner. Physiologically, MBOAT7-mediated LD size reduction activates the AMPK-LXR axis, enhancing cholesterol excretion (Figure 8K).

Living cells are dynamic and complicated metabolic systems where many enzymes form complexes to provide metabolic control, prevent intermediate loss, and enhance catalytic efficiency [35]. This organization is achieved through the spatial and temporal arrangement of enzymes. Compartmentalization of functionally related proteins enhances the overall cellular efficiency, accuracy and specificity, while disruption of this organization can lead to reduced productivity, toxic product accumulation, and protein mislocalization [35]. Previous studies demonstrated that PI-AA, a product of MBOAT7 catalytic activity, inhibits CDS2 activity [10-12]. Thus, our finding that CDS2 binds to MBOAT7 provides a prime example of coordination between enzymes, enabling efficient inhibition of CDS2 activity by PI-AA generated from MBOAT7.

Loss of function of MBOAT7 exacerbates hepatic steatosis, liver inflammation and fibrosis, thus promoting the development of MASLD [11,12,23,25]. Here, we discovered a new role of MBOAT7 in regulating LD dynamics by competing with DGAT2 for binding to RAB1. In MASLD mouse liver, MBOAT7 is more concentrated on LDs compared to normal mouse liver, suggesting that LD-localized MBOAT7 may be involved in the pathogenesis of this disease. We observed that MBOAT7 is typically localized to the ER in wild-type cells but locates to the ER-LD contacts in CDS2 KO cells. The two competitive interactions—between CDS2 and RAB1 for binding to MBOAT7, and between MBOAT7 and DGAT2 for binding to RAB1—are the key underlying molecular mechanisms. MBOAT7 consists of 11 transmembrane domains and lacks the typical features of LD-associated proteins, such as hydrophobic hairpins or amphipathic helices, which allow binding to the phospholipid monolayer or LD surface. Our findings suggest that MBOAT7 localizes

to ER-LD contacts rather than the LD surface. Our study demonstrates that in the absence of CDS2, MBOAT7 is dissociated from the MBOAT7-CDS2 complex and relocates to the ER-LD contacts with the assistance of RAB1.

The competition between MBOAT7 and DGAT2 for binding to RAB1 provides a framework for understanding LD dynamics in the liver. CDS2 deficiency consistently results in "supersized" LDs across various systems [9,13-15,36]. Interestingly, we found that MBOAT7 expression reduces the size of LDs specifically in CDS2-deficient cells, a process that appears independent of MBOAT7 enzymatic activity. Previous research indicates that the increased LD size in CDS2-deficient cells is caused by enhanced targeting of the triglyceride synthesis enzymes DGAT2 and GPAT4 to LDs, a process mediated by RAB1 [14,20,31]. Our findings reveal that MBOAT7 competes with DGAT2 for binding to RAB1, thereby counteracting the effect of DGAT2 on LD size. However, this competition only occurs when CDS2 is absent, suggesting that RAB1 has a stronger binding affinity for DGAT2 than for MBOAT7. While MBOAT7 prevents DGAT2 from associating with LDs in CDS2 KO cells, it does not affect targeting of GPAT4 to LDs, and therefore GPAT4 promotes LD growth in these cells.

MBOAT7 or CDS2 deficiency is linked to the development of MASLD. Recent evidence associates loss of MBOAT7 function with increased plasma cholesterol uptake, which activates the TAZ pathway. This leads to hepatic cholesterol accumulation, inflammation, and progression to MASH [11]. Our data demonstrate that knockdown of *Mboat7* or *Cds2* results in hepatic cholesterol accumulation, likely due to diminished cholesterol excretion via the AMPK-LXR axis. LDs communicate through signaling pathways to regulate a variety of cellular processes. Changes in LD size often accompany lipid accumulation or lipolysis. Evidence suggests that reducing LD size triggers an energy-consuming futile cycle of triglyceride hydrolysis and resynthesis, raising AMP levels and activating AMPK signaling [34]. AMPK activation enhances fatty acid oxidation and cholesterol excretion, which helps remove toxic free fatty acids and free cholesterol, thereby safeguarding liver health. Notably, MBOAT7 loss-of-function mutation is associated with MASLD across various populations [23,37], highlighting AMPK pathway activation as a potential therapeutic strategy for

MBOAT7 deficiency-related MASLD. In summary, our findings demonstrate that MBOAT7 and CDS2 regulate LD size and cholesterol content, and show that LD dynamics controls cholesterol content through the AMPK-LXR axis.

Material and Methods

Mice

Cds2$^{f/f}$ and *Cds2*$^{f/f}$*;AlbCre* mice were generated as described [13]. C57BL/6J mice were purchased from GemPharmatech Co., Ltd. For liver-specific gene knockdowns, C57BL/6J mice were injected with AAV-TBG-sh*Con*, AAV-TBG-sh*Mboat7*, AAV-TBG-sh*Cds2* intravenously (i.v) with $3x10^{11}$ genomic copies of AAVs. The target sequence for *Mboat7* is 5'-CCTGTTGGCTTCCTCTTTAAG-3'. The target sequence for *Cds2* is 5'-GTCCGAAGCAAAGCTAGAT-3'. The control sequence is 5'-GAAGTCGTGAGAAGTAGAA-3'. For liver-specific overexpression of *Mboat7*, C57BL/6J mice were injected with AAV-TBG-*Con* or AAV-TBG-*Mboat7* intravenously (i.v) with $1x10^{11}$ genomic copies of AAVs. Mice were housed at room temperature (22°C) and fed a standard rodent chow diet (Beijing HFK Bioscience Co., Ltd #1032). Unless otherwise stated, 8-week-old male mice were used and all mice were fasted for 5-6 hours prior to euthanization. In some experiments, C57BL/6J mice were fed a chow or GAN diet (Research Diets Inc, D09100310) for 26 weeks. All animal experiments were approved by the Institutional Animal Care and Use Committee (IACUC) at the Institute of Genetics and Developmental Biology, Chinese Academy of Sciences (IGDB-CAS).

Cell culture

The *CDS2* knockout HeLa cell line was generated using the CPISPR/Cas9 system according to published literature [38]. The target sequence was 5'-TATTTACTGAGAATCCGCAA-3'. HepG2 cells (ATCC, HB-8065) and HeLa cells were cultured in DMEM with 10% FBS. In certain experiments, HeLa cells were transfected with siRNAs. The targeting sequence for RAB1A is 5'-CAGCATGAATCCCGAATAT-3'. The targeting sequence for CDS2 is 5'-GGCCACCTTTGTCAATGTA-3'. Mouse primary hepatocytes were isolated from

Cds2$^{f/f}$ and *Cds2*$^{f/f}$*;AlbCre* mice and infected with Ad-EGFP or Ad-MBOAT7-EGFP with MOI=50. All cells were grown at 37°C in a 5% CO_2 incubator.

Plasmids

Human *MBOAT7* cDNA was cloned into the *pcDNA3.1-EGFP* and *pCMV-C-mCherry* vectors. Human *MBOAT5* was cloned into the *pcDNA3.1-EGFP* vector. Human *CDS2* cDNA was cloned into the *pCMV-Tag2b* and *pCS2-HA* vectors. Human *RAB1A*, *DGAT2* and *GPAT4* cDNAs were cloned into both the *pEGFP-N1* and *pCMV-Tag2b* vectors. For His pulldown assays, human *MBOAT7* cDNA was cloned into the *pET-28a* vector.

MBOAT7 activity assay

The activity of MBOAT7 was measured as described with minor modifications [26]. Briefly, 100 μg of protein from liver was incubated in 200 μl of medium (10 mM Tris/HCl, pH 7.5, 150 mM NaCl, 1 mM EDTA) with 50 μM lysophosphatidylinositol (LPI), 25 μM arachidonoyl-CoA (20:4-CoA), and 5 μM (0.2 μCi) radiolabeled arachidonoyl[1-14C]CoA. The reaction was incubated for 15-30 minutes at 37 □C and then stopped by adding 1 mL of chloroform:methanol (2:1, vol/vol) and 0.4 mL of 2% orthophosphoric acid. After centrifugation (3,500 g, 15 min, 4 □C), the lower organic phase, containing the lipids, was collected and dried under a gentle nitrogen stream. Lipids were reconstituted in chloroform. Total lipids were extracted using the Bligh and Dyer method and separated by one-dimensional TLC on silica gel 60 plates using chloroform/methyl acetate:1-propanol:methanol:0.25% KCl (25:25:25:10:9, vol/vol). The radioactivity in the separated bands were quantified using a Typhoon FLA 9000 (GE Healthcare Japan). The corresponding areas of radiolabeled phospholipids on TLC plates were cut out, and the radiolabeled products were measured by liquid scintillation counting.

Lipid analysis

Lipids were extracted based on the chloroform/methanol (2:1, v/v) lipid extraction method (3). In brief, 50 mg of liver tissue were extracted with 6 mL of chloroform/methanol (2:1, v/v), then vortexed and refrigerated overnight. 3 mL of 0.043% magnesium chloride was then added to separate the aqueous phase from the

chloroform phase which contains the lipids. After separation of the two phases, the upper water/methanol phase was removed. A 0.5-mL aliquot of the bottom phase was combined with 1 mL of 0.5% Triton X-100 in chloroform and dried. Triglyceride and total cholesterol levels were measured using commercially available kits (BioSino, Beijing, China). Plasma free fatty acids (FFA) were measured using commercially available kits (Sigma-Alrich, MAK044).

Immunoprecipitation

Cells were transfected with the indicated plasmids using Lipofectamine 3000 (ThermoFisher, L3000001). Proteins were extracted using RIPA lysis buffer, containing100 mM Tris Base, 1% deoxycholate, 0.1% SDS, 5 mM EDTA, 1% Triton-X-100, 150 mM NaCl, pH 8.0), supplemented with 100 mM PMSF, protease inhibitor cocktail (Roche, P8340) and 100 mM sodium vanadate. Lysates were incubated on ice for 15 min, then centrifuged at 12,000 rpm for 15 minutes at 4 °C. Supernatants were incubated overnight at 4 °C with anti-Flag M2 affinity gel (Sigma-Aldrich, A2220) or anti-GPF agarose beads (Lablead Biotech Co., Ltd). After four washes with lysis buffer, beads were denatured in 2X SDS sample buffer for 10 min at 100 °C for western blotting. For the pulldown assay, MBOAT7-His was pulled down using Ni-NTA agarose beads (Qiagen, 30210), then washed three times with PBS + PMSF + 1% Triton buffer. 10 μg of *Flag-CDS2* was expressed in 293T cells, immunoprecipitated using anti-Flag M2 affinity gel, and eluted with 3X Flag peptide. The eluted Flag-CDS2 (1.5 mL) was then incubated with the Ni-NTA agarose-bound MBOAT7-His for 2 hours. The immunoprecipitate was washed six times with PBS + PMSF + 1% Triton buffer and denatured with 2X SDS sample buffer for 10 min before western blotting.

Confocal imaging

The images were acquired using a LSM 980 with Airyscan 2 (Zeiss) or a confocal microscope (Leica SP8). Images were analyzed by Image J.

Subcellular fractionation

Subcellular fractionation of liver tissue was performed as described [39].

Antibodies

Rabbit antibodies against CDS2 (1:500, 13175-1-AP), SREBP2 (1:1000, 28212-1-AP), LDLR (1:1000, 10785-1-AP), SR-B1 (1:1000, 21277-1-AP) and MBOAT7 (1:100, 83546-3-RR) were purchased from Proteintech. Rabbit antibody against MBOAT7 (1:1000, AV49811) was purchased from Sigma-Aldrich. Mouse antibody against Flag (1:1000, F1804) was purchased from Sigma-Aldrich. Rabbit antibody against Flag (1:2500, PM020) was purchased from MBL. Rabbit antibodies against ATGL (1:1000, 2138), phospho-AMPKα(Thr172)(40H9) (1:1000, 2535), AMPKα (1:1000, 2532), phospho-ACC (1:1000, 3661), ACC (1:1000, 3662), and ABCA1 (1:1000, 96292) were purchased from Cell Signaling. Mouse antibody against LXR (1:1000, ab41902) was purchased from Abcam. Rabbit antibodies against DGAT2 (1:1000, ab237613) and HMGCR (1:1000, ab174830) were purchased from Abcam.

Statistics

Results with error bars are mean±SEM. Comparisons between 2 groups were performed using the two-tailed Student's t-test. ANOVA was used for comparisons between more than 2 groups.

Acknowledgments

We thank Xixian Li from the Center for Biological Imaging at the Institute of Biophysics, CAS, for analyzing images. This work was supported by grants 2024YFA1306101, 2023YFA1800500 from National Key R&D Program of China and 92354301, 32230044, 32371230 and 32321004 from the National Natural Science Foundation of China, and BJ-2024-235 from National High Level Hospital Clinical Research Funding.

Figure 4A, Figure 6I and Figure 8Kwere created with BioRender (*https://BioRender.com/ k88h902*, *https://BioRender.com/s73x778, and https://BioRender.com/e57c295*).

Declaration of Interests

The authors have declared that no conflict of interest exists.

Author Contributions

J Xu and X Huang designed the experiments. J Xu, J Zhang, W Wang and H Su

performed the experiments. J Xu, J Zhang, S Chen and M Ding analyzed the data. J Xu and X Huang wrote the manuscript.

References

1 Llovet, J. M. *et al.* Nonalcoholic steatohepatitis-related hepatocellular carcinoma: pathogenesis and treatment. *Nat Rev Gastro Hepat* **20**, 487-503, doi:10.1038/s41575-023-00754-7 (2023).

2 Xiang, L. *et al.* A multi-omic landscape of steatosis-to-NASH progression. *Life Metab* **1**, 242-257, doi:10.1093/lifemeta/loac034 (2022).

3 Linden, D. & Romeo, S. Therapeutic opportunities for the treatment of NASH with genetically validated targets. *J Hepatol* **79**, 1056-1064, doi:10.1016/j.jhep.2023.05.007 (2023).

4 Buch, S. *et al.* A genome-wide association study confirms PNPLA3 and identifies TM6SF2 and MBOAT7 as risk loci for alcohol-related cirrhosis. *Nat Genet* **47**, 1443-1448, doi:10.1038/ng.3417 (2015).

5 Thangapandi, V. R. *et al.* Loss of hepatic Mboat7 leads to liver fibrosis. *Gut* **70**, 940-950, doi:10.1136/gutjnl-2020-320853 (2021).

6 Varadharajan, V., Massey, W. J. & Brown, J. M. Membrane-bound O-acyltransferase 7 (MBOAT7)-driven phosphatidylinositol remodeling in advanced liver disease. *J Lipid Res* **63**, 100234, doi:10.1016/j.jlr.2022.100234 (2022).

7 Alharthi, J. *et al.* A metabolic associated fatty liver disease risk variant in MBOAT7 regulates toll like receptor induced outcomes. *Nat Commun* **13**, 7430, doi:10.1038/s41467-022-35158-9 (2022).

8 Caddeo, A., Spagnuolo, R. & Maurotti, S. MBOAT7 in liver and extrahepatic diseases. *Liver Int* **43**, 2351-2364, doi:10.1111/liv.15706 (2023).

9 Liu, Y., Wang, W., Shui, G. & Huang, X. CDP-diacylglycerol synthetase coordinates cell growth and fat storage through phosphatidylinositol metabolism and the insulin pathway. *PLoS Genet* **10**, e1004172, doi:10.1371/journal.pgen.1004172 (2014).

10 D'Souza, K., Kim, Y. J., Balla, T. & Epand, R. M. Distinct properties of the two isoforms of CDP-diacylglycerol synthase. *Biochemistry* **53**, 7358-7367, doi:10.1021/bi501250m (2014).

11 Moore, M. P. *et al.* Low MBOAT7 expression, a genetic risk for MASH, promotes a profibrotic pathway involving hepatocyte TAZ upregulation. *Hepatology* **81**, 576-590, doi:10.1097/HEP.0000000000000933 (2024).

12 Tanaka, Y. *et al.* LPIAT1/MBOAT7 depletion increases triglyceride synthesis fueled by high phosphatidylinositol turnover. *Gut* **70**, 180-193, doi:10.1136/gutjnl-2020-320646 (2021).

13 Xu, J. *et al.* Hepatic CDP-diacylglycerol synthase 2 deficiency causes mitochondrial dysfunction and promotes rapid progression of NASH and fibrosis. *Sci Bull (Beijing)* **67**, 299-314, doi:10.1016/j.scib.2021.10.014 (2022).

14 Xu, Y. *et al.* CDP-DAG synthase 1 and 2 regulate lipid droplet growth through distinct mechanisms. *J Biol Chem* **294**, 16740-16755, doi:10.1074/jbc.RA119.009992 (2019).

15 Qi, Y. *et al.* CDP-diacylglycerol synthases regulate the growth of lipid droplets and adipocyte development. *J Lipid Res* **57**, 767-780, doi:10.1194/jlr.M060574 (2016).

16 Walther, T. C., Chung, J. & Farese, R. V., Jr. Lipid Droplet Biogenesis. *Annu Rev Cell Dev Biol* **33**,

491-510, doi:10.1146/annurev-cellbio-100616-060608 (2017).

17 Poppelreuther, M. *et al.* The metabolic capacity of lipid droplet localized acyl-CoA synthetase 3 is not sufficient to support local triglyceride synthesis independent of the endoplasmic reticulum in A431 cells. *Biochim Biophys Acta Mol Cell Biol Lipids* **1863**, 614-624, doi:10.1016/j.bbalip.2018.03.003 (2018).

18 Zechner, R. FAT FLUX: enzymes, regulators, and pathophysiology of intracellular lipolysis. *EMBO Mol Med* **7**, 359-362, doi:10.15252/emmm.201404846 (2015).

19 Olarte, M. J. *et al.* Determinants of Endoplasmic Reticulum-to-Lipid Droplet Protein Targeting. *Dev Cell* **54**, 471-487 doi:10.1016/j.devcel.2020.07.001 (2020).

20 Song, J. *et al.* Identification of two pathways mediating protein targeting from ER to lipid droplets. *Nat Cell Biol* **24**, 1364-1377, doi:10.1038/s41556-022-00974-0 (2022).

21 Xu, D. *et al.* Rab18 promotes lipid droplet (LD) growth by tethering the ER to LDs through SNARE and NRZ interactions. *J Cell Biol* **217**, 975-995, doi:10.1083/jcb.201704184 (2018).

22 Kumar, A., Yadav, S. & Choudhary, V. The evolving landscape of ER-LD contact sites. *Front Cell Dev Biol* **12**, 1483902, doi:10.3389/fcell.2024.1483902 (2024).

23 Mancina, R. M. *et al.* The MBOAT7-TMC4 Variant rs641738 Increases Risk of Nonalcoholic Fatty Liver Disease in Individuals of European Descent. *Gastroenterology* **150**, 1219-1230 e1216, doi:10.1053/j.gastro.2016.01.032 (2016).

24 Bezawork-Geleta, A. *et al.* Proximity proteomics reveals a mechanism of fatty acid transfer at lipid droplet-mitochondria- endoplasmic reticulum contact sites. *Nat Commun* **16**, 2135, doi:10.1038/s41467-025-57405-5 (2025).

25 Meroni, M. *et al.* Mboat7 down-regulation by hyper-insulinemia induces fat accumulation in hepatocytes. *EBioMedicine* **52**, 102658, doi:10.1016/j.ebiom.2020.102658 (2020).

26 Wang, K. *et al.* The structure of phosphatidylinositol remodeling MBOAT7 reveals its catalytic mechanism and enables inhibitor identification. *Nat Commun* **14**, 3533, doi:10.1038/s41467-023-38932-5 (2023).

27 Dhiman, R., Caesar, S., Thiam, A. R. & Schrul, B. Mechanisms of protein targeting to lipid droplets: A unified cell biological and biophysical perspective. *Semin Cell Dev Biol* **108**, 4-13, doi:10.1016/j.semcdb.2020.03.004 (2020).

28 Pataki, C. I. *et al.* Proteomic analysis of monolayer-integrated proteins on lipid droplets identifies amphipathic interfacial alpha-helical membrane anchors. *Proc Natl Acad Sci U S A* **115**, E8172-E8180, doi:10.1073/pnas.1807981115 (2018).

29 Bersuker, K. *et al.* A Proximity Labeling Strategy Provides Insights into the Composition and Dynamics of Lipid Droplet Proteomes. *Dev Cell* **44**, 97-112 e117, doi:10.1016/j.devcel.2017.11.020 (2018).

30 Mejhert, N. *et al.* Partitioning of MLX-Family Transcription Factors to Lipid Droplets Regulates Metabolic Gene Expression. *Mol Cell* **77**, 1251-1264 e1259, doi:10.1016/j.molcel.2020.01.014 (2020).

31 Malis, Y. *et al.* Rab1b facilitates lipid droplet growth by ER-to-lipid droplet targeting of DGAT2. *Sci Adv* **10**, eade7753, doi:10.1126/sciadv.ade7753 (2024).

32 Wilfling, F. *et al.* Triacylglycerol synthesis enzymes mediate lipid droplet growth by relocalizing from the ER to lipid droplets. *Dev Cell* **24**, 384-399, doi:10.1016/j.devcel.2013.01.013 (2013).

33 Wang, J. Q. *et al.* Inhibition of ASGR1 decreases lipid levels by promoting cholesterol

excretion. *Nature* **608**, 413-420, doi:10.1038/s41586-022-05006-3 (2022).

34 Chen, G., Zhou, G., Lotvola, A., Granneman, J. G. & Wang, J. ABHD5 suppresses cancer cell anabolism through lipolysis-dependent activation of the AMPK/mTORC1 pathway. *J Biol Chem* **296**, 100104, doi:10.1074/jbc.RA120.014682 (2021).

35 Bar-Peled, L. & Kory, N. Principles and functions of metabolic compartmentalization. *Nat Metab* **4**, 1232-1244, doi:10.1038/s42255-022-00645-2 (2022).

36 Mak, H. Y. *et al.* AGPAT2 interaction with CDP-diacylglycerol synthases promotes the flux of fatty acids through the CDP-diacylglycerol pathway. *Nat Commun* **12**, 6877, doi:10.1038/s41467-021-27279-4 (2021).

37 Xu, X. *et al.* MBOAT7 rs641738 (C>T) is associated with NAFLD progression in men and decreased ASCVD risk in elder Chinese population. *Front Endocrinol (Lausanne)* **14**, 1199429, doi:10.3389/fendo.2023.1199429 (2023).

38 Ran, F. A. *et al.* Genome engineering using the CRISPR-Cas9 system. *Nat Protoc* **8**, 2281-2308, doi:10.1038/nprot.2013.143 (2013).

39 Ding, Y. *et al.* Isolating lipid droplets from multiple species. *Nat Protoc* **8**, 43-51, doi:10.1038/nprot.2012.142 (2013).

Figure Legends

Figure 1. MBOAT7 and CDS2 regulate lipid metabolism in liver.

(A-B) The correlation between *MBOAT7* and *CDS2* transcript levels in the gene expression datasets GSE48452 (NASH samples) and GSE66676, respectively. (C) The correlation between *MBOAT7* and *CDS2* transcript levels in the GEPIA website. (D-F) Procedure for liver-specific knockdown of *Mboat7* and/or *Cds2* in mice. Mice were injected with AAV-TBG-shCon, AAV-TBG-sh*Mboat7*, AAV-TBG-sh*Cds2*, or AAV-TBG-sh*Mboat7* + AAV-TBG-sh*Cds2* and fed a chow diet for 4 weeks before analysis. (D). Hepatic triglyceride (E) and cholesterol (F) levels were measured in the mice in (D). N=6-7 mice per group. (G) H&E staining of liver sections from mice in (D). Scale bar represents 50 μm in main images and 10 μm in enlarged images. (H) Hepatic steatosis score based on liver sections of mice in (D). N=6-7 mice per group. (I) RNAseq was performed on liver samples from the mice in (D). The numbers of genes up- or down-regulated in sh*Mboat7* vs sh*Con*, sh*Cds2* vs sh*Con* and sh*Mboat7* + sh*Cds2* vs sh*Con* are shown. (J) KEGG analysis results showing the pathways related to the 301 common downregulated genes in (I). (K) qRT-PCR analysis of the mRNA levels of genes that regulate cholesterol and fatty acid metabolism in the liver. N=5-8 mice per group. (L) Western blot analysis of liver lysates from mice in (D).

N=3 mice per group. * $p < 0.05$, ** $p < 0.01$, *** $p < 0.001$.

Figure 2. MBOAT7 is localized to the ER-LD contacts in CDS2 KO cells.
(A) CDS2 KO and control HeLa cells were transfected with MBOAT7-EGFP and treated with 100 μM OA for 12 hours, followed by LD labeling with LipidTOX. (B) Fluorescence colocalization was analyzed along the white line in the main confocal image. (C) CDS2 KO and control HeLa cells were treated with 100 μM OA for 12 hours and immunostained with anti-MBOAT7 antibody. (D) Fluorescence colocalization was analyzed along the white line in the main confocal image. (E) A 3D-SIM image reveals that MBOAT7-EGFP enwraps a LD in an OA-treated CDS2 KO cell. Scale bar: 2 μm. (F) CDS2 KO and control HeLa cells were transfected with mCherry-SEC61b (an ER marker), then treated with 100 μM OA for 12 hours. LDs were labeled with BODIPY. (G) Fluorescence colocalization was analyzed along the white line in the main confocal image. (H) C56BL/6 mice were fed a chow (control) or GAN (MASLD) diet (40 kcal% fat, 20 kcal% fructose and 2% cholesterol) for 26 weeks. Liver sections were immunostained with anti-MBOAT7 antibody. White arrows indicate MBOAT7 enclosing LDs. (I) The number of LDs surrounded by MBOAT7 was quantified by analyzing 1,000 LDs in confocal images. N=9-11 liver sections per group. Except for (E), scale bars represent 10 μm in main images and 2 μm in enlarged images.

Figure 3. The N-terminus of MBOAT7 is essential for LD targeting of MBOAT7 and MBOAT7 interacts with CDS2.
(A) Top: 3D structure of MBOAT7 in the ER membrane, highlighting its transmembrane (TM) domains. Bottom: The 11 TM domains of MBOAT7 (boxes) and the three regions of the protein expressed as truncations. (B) CDS2 KO cells transfected with truncated versions of MBOAT7 were treated with 100 μM OA for 12 hours, followed by LD labeling with LipidTOX. (C) CDS2 KO cells transfected with MBOAT7-EGFP containing specific TM domain deletions were treated with 100 μM OA for 12 hours. LDs were labeled with LipidTOX. (D) CDS2 KO cells transfected

with MBOAT7-EGFP chimeras containing TM3 or TM4 from MBOAT5 were treated with 100 μM OA for 12 hours and labeled with LipidTOX to stain LDs. (E) Co-IP assay showing that Flag-CDS2 precipitates MBOAT7-EGFP. (F) Co-IP assay showing that MBOAT7-EGFP precipitates Flag-CDS2. (G) Co-IP assay demonstrating that endogenous CDS2 precipitates MBOAT7. (H) *In vitro* pull-down assay indicating that Flag-CDS2 directly binds to MBOAT7-His. Scale bars: 10 μm in main images and 2 μm in enlarged images.

Figure 4. RAB1 is required for targeting of MBOAT7 to LDs in CDS2 KO cells.
(A) Schematic of the workflow for identifying MBOAT7-interacting proteins in control and CDS2 KO cells. (B) Venn diagram illustrating the overlap between the MBOAT7-interacting proteins from (A) and LD proteins from various LD proteomes. (C) Five MBOAT7-interacting proteins identified from the Venn diagram in (B). (D) CDS2 KO cells were transfected with siNC or siRAB1A, and MBOAT7-EGFP, then treated with 100 μM OA for 12 hours. LDs were labeled with LipidTOX. (E) *RAB1A* mRNA levels in HeLa cells transfected with control siRNA or siRAB1A. (F) Quantification of LDs surrounded by MBOAT7-EGFP in control (siNC) or RAB1A knockdown (siRAB1A) cells. (G) Co-IP assay showing that Flag-RAB1A precipitates MBOAT7-EGFP in CDS2 KO cells. (H) Co-IP assay showing that Flag-RAB1A precipitates MBOAT7-EGFP in CDS2 KO cells, and expression of HA-CDS2 in CDS2 KO cells disrupts the RAB1A/MBOAT7 interaction. (I) 3D structure of MBOAT7/RAB1A docking and the potential binding sites. (H) Co-IP assay showing that Flag-RAB1A precipitates MBOAT7-EGFP, but fails to interact with MBOAT7-BS-mut-EGFP, in which the RAB1A-binding sites are mutated in CDS2 KO cells.

Figure 5. MBOAT7 reduces LD size in CDS2 KO cells by competing with DGAT2 for targeting to LDs.
(A) Control HeLa or CDS2 KO cells were transfected with MBOAT7-EGFP or the MBOAT7(N321A, H356A)-EGFP mutant, then treated with 100 μM OA for 12 hours.

LDs were labeled by LipidTOX. Scale bar: 10 μm. (B) Quantification of LD sizes from (A). N=200 per group. (C) 293T cells were transfected with GFP-RAB1A and Flag-DGAT2 or Flag control plasmids. Co-IP assay shows that Flag-DGAT2 precipitates GFP-RAB1A. (D) 293T cells were transfected with GFP-RAB1A and Flag-GPAT4 or Flag control plasmid. Co-IP assay shows that Flag-GPAT4 precipitates GFP-RAB1A. (E) CDS2 KO cells were transfected with GFP-RAB1A and Flag-DAGT2 with or without MBOAT7-EGFP. Co-IP shows that Flag-DGAT2 precipitates GFP-RAB1A. (F) CDS2 KO cells were transfected with Flag-DGAT2 and GFP-RAB1A with siRNA control (siCon) or siMBOAT7. Co-IP assay shows that Flag-DGAT2 precipitates GFP-RAB1A. (G) Confocal images showing that EGFP-DGAT2 targets to LDs in CDS2 KO cells. MBOAT7-mCherry expression blocks LD targeting of DGAT2. Scale bar: 10 μm in main images and 2 μm in enlarged images. (H) Co-IP assay showing that Flag-DGAT2 precipitates full-length GFP-RAB1A as well as N-terminal and C-terminal truncated forms. (I) Co-IP assay showing that Flag-MBOAT7 precipitates full length GFP-RAB1A as well as N-terminal and C-terminal truncated forms. (J) Co-IP assay showing that Flag-DGAT2 precipitates GFP-RAB1A in CDS2 KO cells treated with or without OA. (K) Co-IP assay showing that Flag-MBOAT7 precipitates GFP-RAB1A in CDS2 KO cells treated with or without OA. **** $p < 0.0001$.

Figure 6. MBOAT7 regulates LD size and lipolysis.

(A) MBOAT7 enzymatic activity was measured in *Cds2*$^{f/f}$, *Cds2*$^{f/f}$*;AlbCre* mice, and *Cds2*$^{f/f}$*;AlbCre* mice injected with AAV-TBG-*Cds2*. N=5-6 mice per group. (B) Schematic showing the procedure for hepatic overexpression of MBOAT7 in the liver of mice with and without hepatic depletion of CDS2. *Cds2*$^{f/f}$ and *Cds2*$^{f/f}$*;AlbCre* mice were injected with AAV-TBG-Con or AAV-TBG-*Mboat7* and fed a chow diet for 4 weeks before analysis. (C and D) Hepatic cholesterol (C) and triglyceride (D) levels were analyzed in the mice from (B). N=7-8 mice per group. (E) H&E staining of liver sections from *Cds2*$^{f/f}$ and *Cds2*$^{f/f}$*;AlbCre* mice. Scale bar represents 50 μm in main images and 10 μm in enlarged images. (F) Primary hepatocytes isolated from *Cds2*$^{f/f}$

and *Cds2*$^{f/f}$*;AlbCre* mice were infected with Ad-EGFP or Ad-MBOAT7-EGFP and treated with 100 μM OA for 12 hours. LDs were stained with LipdTOX before confocal imaging. Scale bar represents 10 μm in main images and 2 μm in enlarged images. (G) Quantification of LD sizes in (F). (H) Western blot analysis of LD, ER and cytosol fractions from the liver of *Cds2*$^{f/f}$*;AlbCre* mice that are injected with AAV-TBG-Con or AAV-TBG-*Mboat7*. (I) Primary hepatocytes from *Cds2*$^{f/f}$ and *Cds2*$^{f/f}$*;AlbCre* mice were infected with Ad-EGFP or Ad-MBOAT7-EGFP, then treated with 10 μM ISO or DMSO (control) for the indicated times. Free fatty acids in the medium were analyzed. * $p < 0.05$, ** $p < 0.01$, *** $p < 0.001$, **** $p < 0.0001$.

Figure 7. MBOAT7 and CDS2 regulate cholesterol metabolism through the AMPK pathway.

(A) Western blot of *Cds2*$^{f/f}$ and *Cds2*$^{f/f}$*;AlbCre* mice injected with AAV-TBG-Con or AAV-TBG-*Mboat7*, and fed a chow diet for 4 weeks before analysis. (B) Quantifications of proteins from (A). (C) qRT-PCR analysis of genes involved in cholesterol and fatty acid metabolism. (D) Primary hepatocytes isolated from *Cds2*$^{f/f}$*;AlbCre* mice were infected with Ad-EGFP or Ad-MBOAT7-EGFP. Cells were serum-starved for 4 hours, then treated with 10 μM dorsomorphin in no-glucose DMEM + 10% FBS medium for 4 hours. Western blot analysis was then performed. (E) Primary hepatocytes from *Cds2*$^{f/f}$*;AlbCre* mice were infected with Ad-EGFP or Ad-MBOAT7-EGFP and treated with 10 μM ISO or DMSO (control) for 6 hours. Western blot analysis was then performed. (F) Quantifications of proteins from (E). (G) Primary hepatocytes from *Cds2*$^{f/f}$*;AlbCre* mice were infected with Ad-EGFP or Ad-MBOAT7-EGFP. Cells were pretreated with DMSO (control) or Atglistatin (ATGLi; 20 μM) for 30 minutes, then treated with 10 μM ISO for 6 hours. Protein levels were analyzed by western blotting. (H) Quantifications of proteins from (H). * $p < 0.05$, ** $p < 0.01$, *** $p < 0.001$, **** $p < 0.0001$.

Figure 8. AMPK agonist ameliorates *Cds2*- or *Mboat7*-deficiency-induced MASLD.

(A) Schematic showing the procedure for sh*Cds2* and sh*Mboat7* mice with or without A769662 treatment. 8-week-old C57BL6/J mice were injected with either AAV-TBG-sh*Cds2* or AAV-TBG-sh[31] and concurrently fed a NASH-inducing GAN diet for 4 weeks. During the final 2 weeks of this period, mice received intraperitoneal injections of the AMPK agonist A769662 (30 mg/kg, twice daily). (B-G) Body weight (B), plasma triglyceride (C) and cholesterol (D), hepatic triglyceride (E) and cholesterol (F), plasma ALT levels (G) were shown. (H) Representative H&E and Oil-Red-O staining for liver sections from the indicated groups in (A). (I) mRNA levels of genes involved in lipogenesis, fatty acid oxidation and cholesterol excretion. (J) Protein levels of key components in the LXR signaling pathway. (H) A model illustrating how MBOAT7 and CDS2 regulate LD dynamics and cholesterol metabolism in hepatocytes. CDS2 and MBOAT7 physically interact in the ER membrane and both regulate PI biosynthesis. MBOAT7 catalyzes the generation of PI-AA, which inhibits CDS2 activity. In the absence of CDS2, MBOAT7 relocates to the ER-LD contacts via binding to RAB1. CDS2 deficiency causes increased LD size accompanied by increased recruitment of DGAT2 to LDs, whereas overexpression of MBOAT7 in CDS2-deficient conditions reduces DGAT2 targeting to LDs, increases ATGL recruitment to the LD surface, and reduces LD size. The increased lipolysis induced by MBOAT7 expression activates AMPK, enhancing LXR protein levels and expression of its downstream target genes, thus stimulating cholesterol metabolism. * * $p < 0.05$, ** $p < 0.01$, *** $p < 0.001$, **** $p < 0.0001$, # $p<0.05$, ## $p<0.01$.

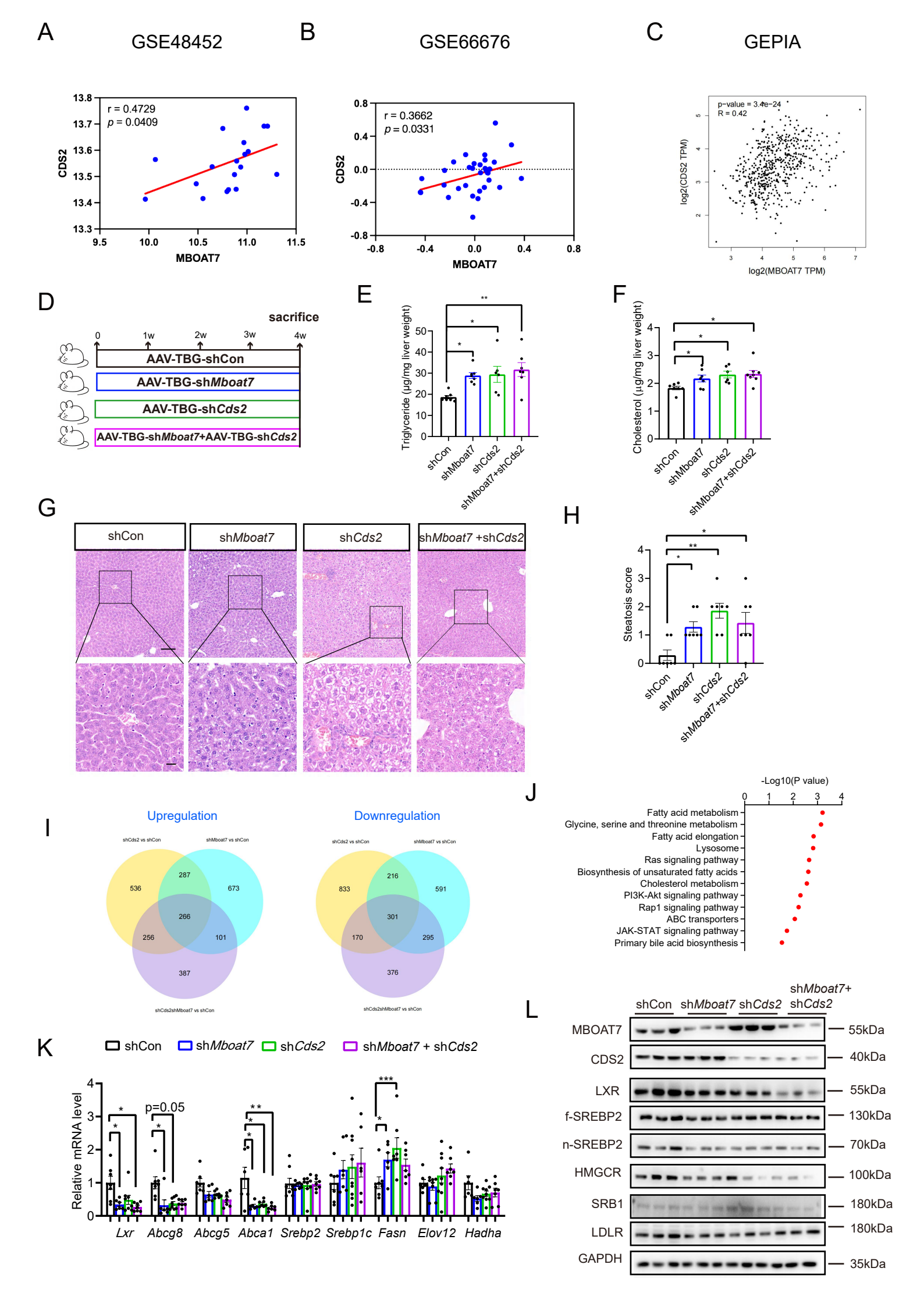
A
GSE48452
r = 0.4729
p = 0.0409
CDS2
MBOAT7
B
GSE66676
r = 0.3662
p = 0.0331
CDS2
MBOAT7
C
GEPIA
p-value = 3.4e-24
R = 0.42
log2(CDS2 TPM)
log2(MBOAT7 TPM)
D
sacrifice
0
1w
2w
3w
4w
AAV-TBG-shCon
AAV-TBG-shMboat7
AAV-TBG-shCds2
AAV-TBG-shMboat7+AAV-TBG-shCds2
E
Triglyceride (μg/mg liver weight)
shCon
shMboat7
shCds2
shMboat7+shCds2
F
Cholesterol (μg/mg liver weight)
shCon
shMboat7
shCds2
shMboat7+shCds2
G
shCon
shMboat7
shCds2
shMboat7 +shCds2
H
Steatosis score
shCon
shMboat7
shCds2
shMboat7+shCds2
I
Upregulation
shCds2 vs shCon
shMboat7 vs shCon
shCds2shMboat7 vs shCon
536
287
673
266
256
101
387
Downregulation
shCds2 vs shCon
shMboat7 vs shCon
shCds2shMboat7 vs shCon
833
216
591
301
170
295
376
J
-Log10(P value)
Fatty acid metabolism
Glycine, serine and threonine metabolism
Fatty acid elongation
Lysosome
Ras signaling pathway
Biosynthesis of unsaturated fatty acids
Cholesterol metabolism
PI3K-Akt signaling pathway
Rap1 signaling pathway
ABC transporters
JAK-STAT signaling pathway
Primary bile acid biosynthesis
K
shCon
shMboat7
shCds2
shMboat7 + shCds2
Relative mRNA level
p=0.05
Lxr
Abcg8
Abcg5
Abca1
Srebp2
Srebp1c
Fasn
Elov12
Hadha
L
shCon
shMboat7
shCds2
shMboat7+ shCds2
MBOAT7
CDS2
LXR
f-SREBP2
n-SREBP2
HMGCR
SRB1
LDLR
GAPDH
55kDa
40kDa
55kDa
130kDa
70kDa
100kDa
180kDa
180kDa
35kDa

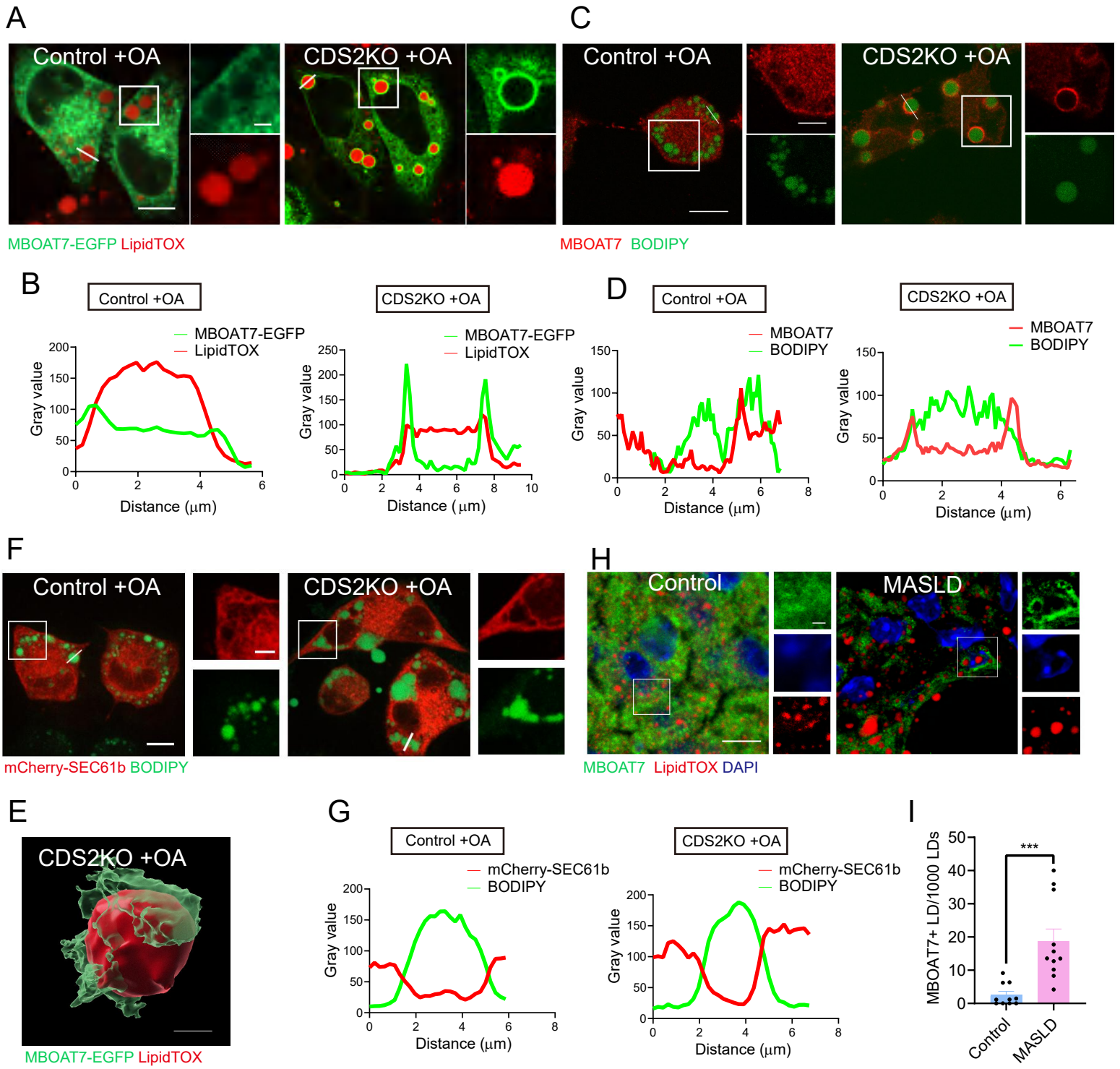
A
Control +OA
CDS2KO +OA
MBOAT7-EGFP LipidTOX
C
Control +OA
CDS2KO +OA
MBOAT7 BODIPY
B
Control +OA
CDS2KO +OA
MBOAT7-EGFP
LipidTOX
Gray value
Distance (μm)
D
Control +OA
CDS2KO +OA
MBOAT7
BODIPY
Gray value
Distance (μm)
F
Control +OA
CDS2KO +OA
mCherry-SEC61b BODIPY
H
Control
MASLD
MBOAT7 LipidTOX DAPI
E
CDS2KO +OA
MBOAT7-EGFP LipidTOX
G
Control +OA
CDS2KO +OA
mCherry-SEC61b
BODIPY
Gray value
Distance (μm)
I
MBOAT7+ LD/1000 LDs
***
Control
MASLD

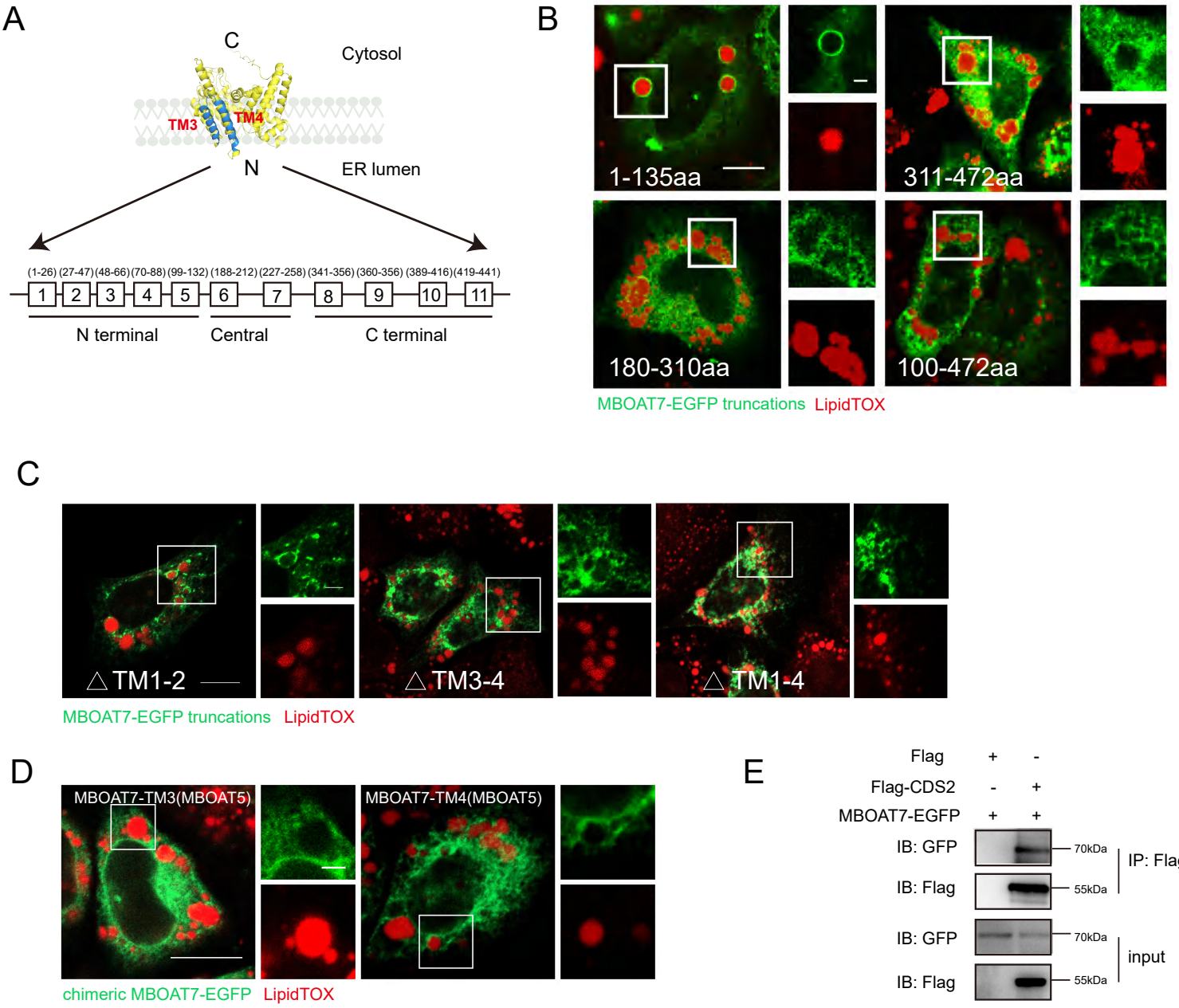
A
C
Cytosol
TM3
TM4
N
ER lumen
(1-26) (27-47) (48-66) (70-88) (99-132) (188-212) (227-258) (341-356) (360-356) (389-416) (419-441)
1 2 3 4 5 6 7 8 9 10 11
N terminal
Central
C terminal
B
1-135aa
311-472aa
180-310aa
100-472aa
MBOAT7-EGFP truncations LipidTOX
C
△TM1-2
△TM3-4
△TM1-4
MBOAT7-EGFP truncations LipidTOX
D
MBOAT7-TM3(MBOAT5)
MBOAT7-TM4(MBOAT5)
chimeric MBOAT7-EGFP LipidTOX
E
Flag + -
Flag-CDS2 - +
MBOAT7-EGFP + +
IB: GFP
IB: Flag
70kDa
55kDa
IP: Flag
input
F
EGFP + -
MBOAT7-EGFP - +
Flag-CDS2 + +
IB: Flag
IB: GFP
55kDa
70kDa
IP: GFP
input
G
Con GFP-CDS2 KI
IB: MBOAT7
IB: GFP
55kDa
70kDa
IP: GFP
input
H
His + -
His-MBOAT7 - +
Flag-CDS2 + +
IB: Flag
IB: His
55kDa
His pulldown
input

A

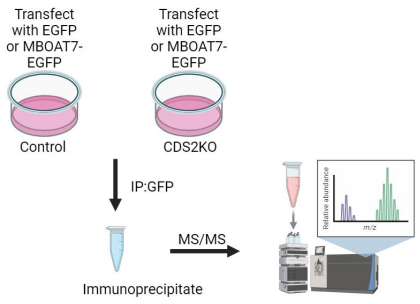

B

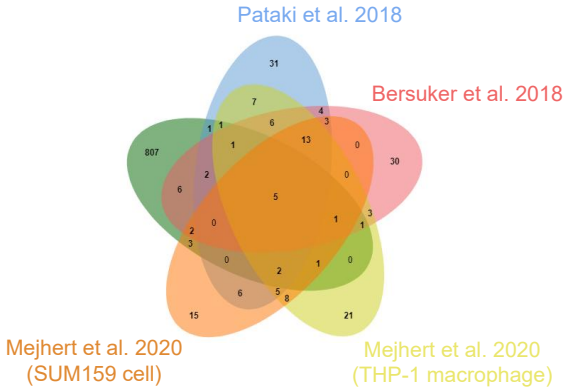

C

Protein	Fold change
RAB7A	10.4
RAB1A	7.2
RAB18	6.2
RAB14	4.8
CYB5R3	4

D

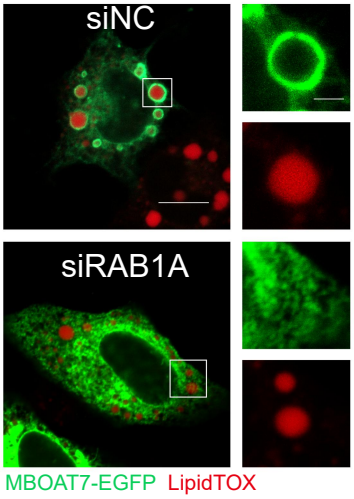

E

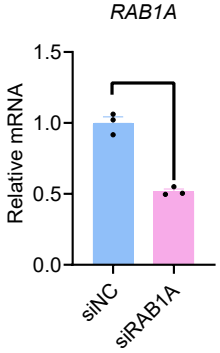

F

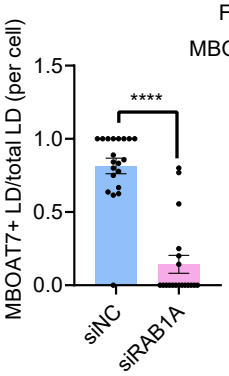

G

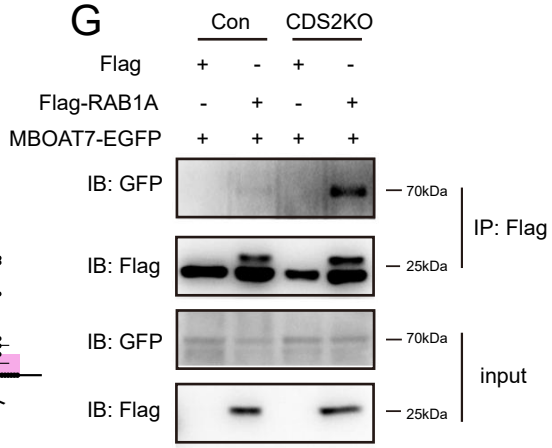

H

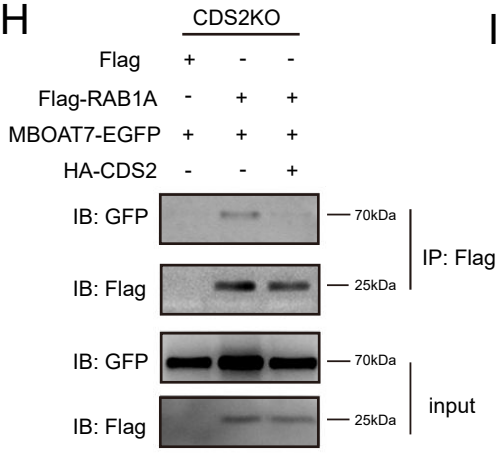

I

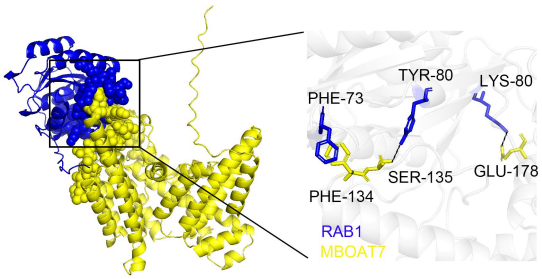

J

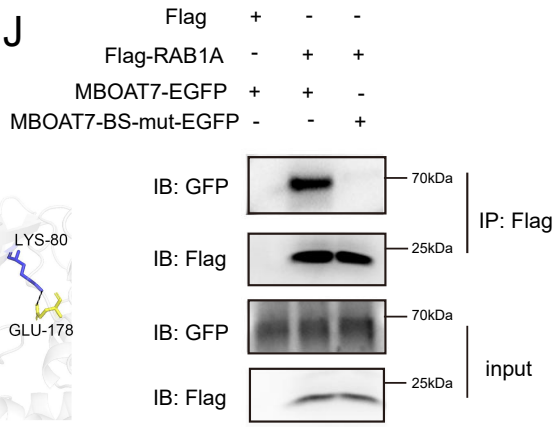

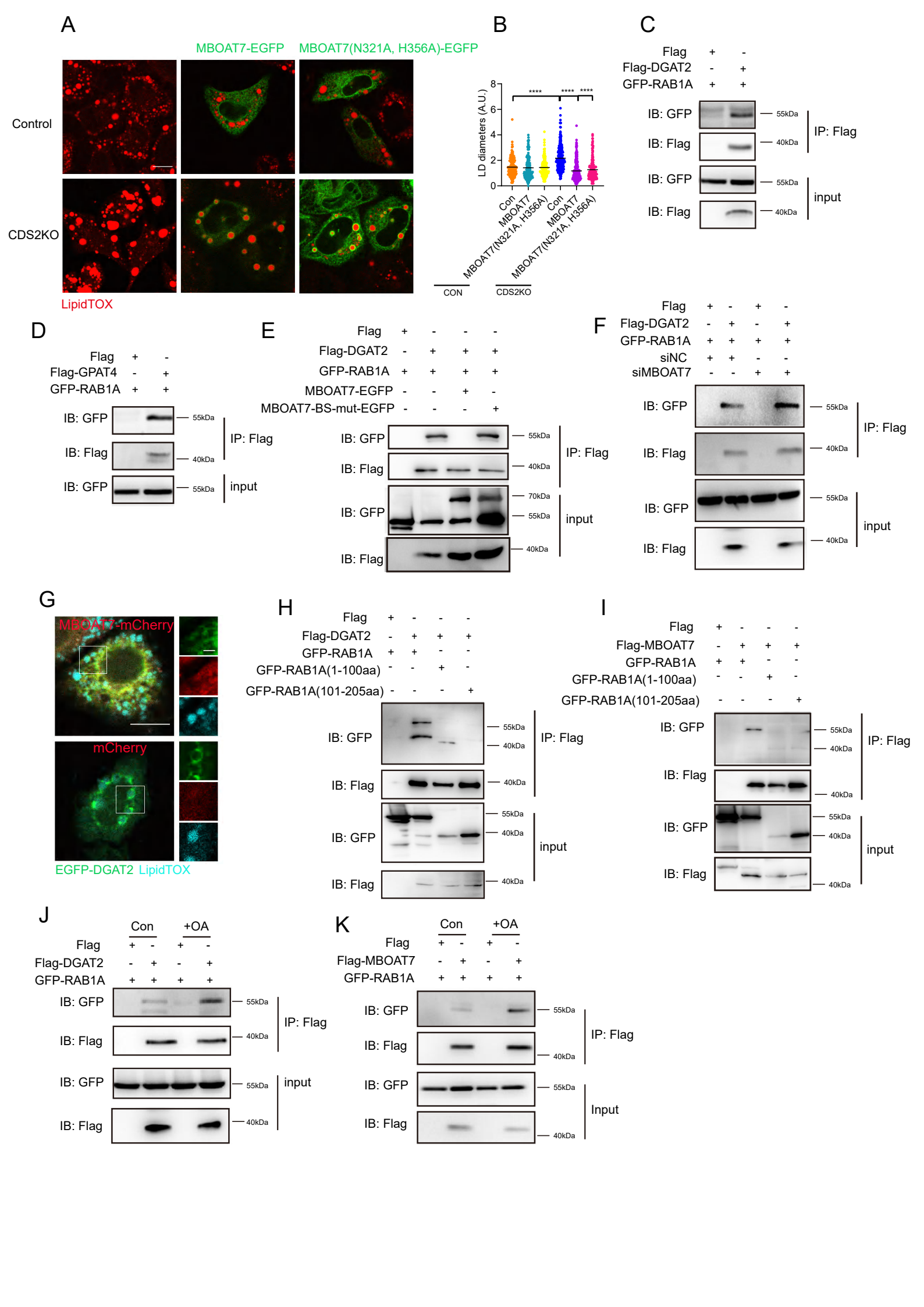
A
MBOAT7-EGFP
MBOAT7(N321A, H356A)-EGFP
Control
CDS2KO
LipidTOX
B
LD diameters (A.U.)
Con
MBOAT7
MBOAT7(N321A, H356A)
CON
CDS2KO
C
Flag
Flag-DGAT2
GFP-RAB1A
IB: GFP
IB: Flag
IP: Flag
input
55kDa
40kDa
D
Flag-GPAT4
E
MBOAT7-EGFP
MBOAT7-BS-mut-EGFP
70kDa
F
siNC
siMBOAT7
G
MBOAT7-mCherry
mCherry
EGFP-DGAT2 LipidTOX
H
GFP-RAB1A(1-100aa)
GFP-RAB1A(101-205aa)
I
Flag-MBOAT7
J
Con
+OA
K
Input

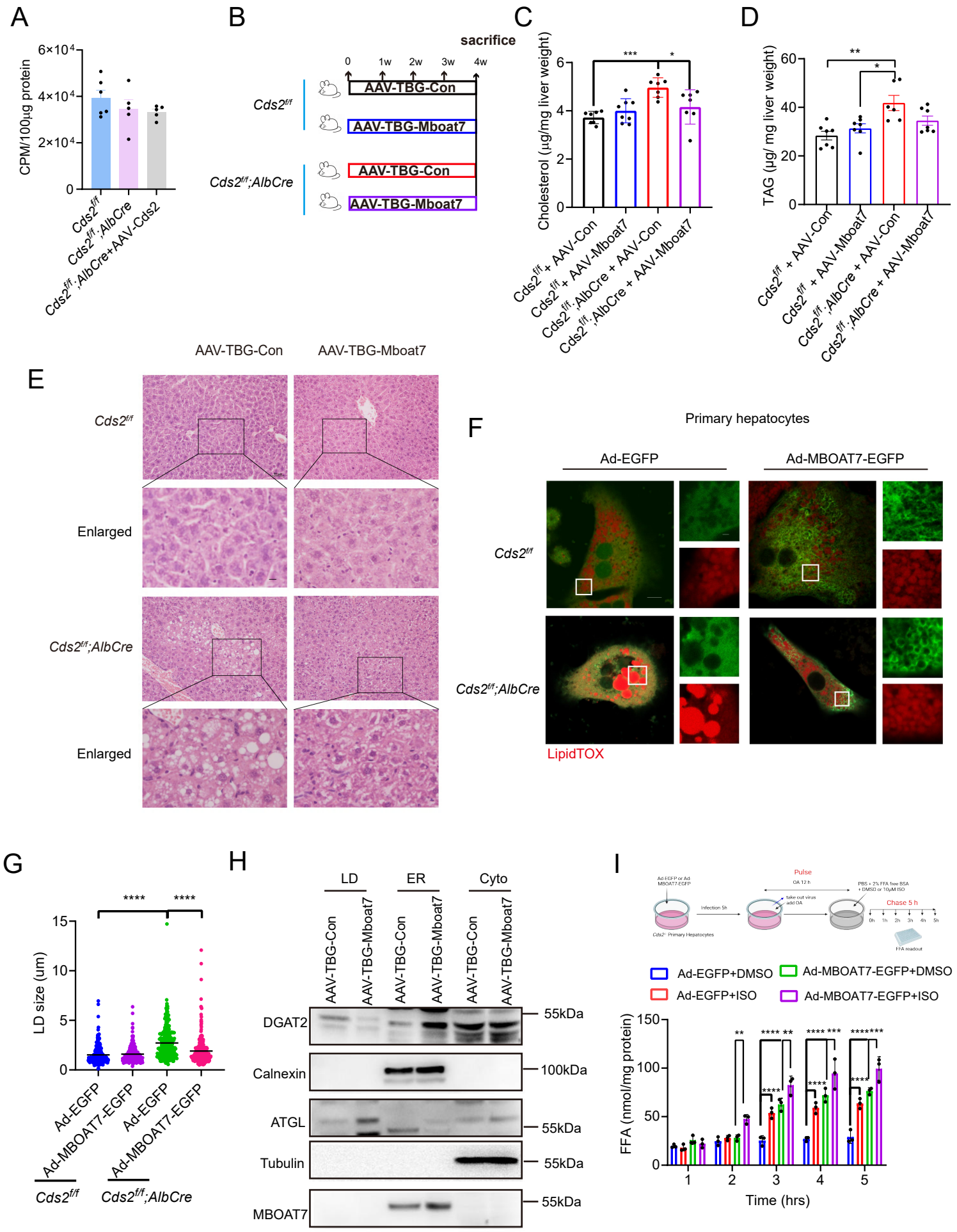
A
CPM/100μg protein
6×10⁴
4×10⁴
2×10⁴
0
Cds2f/f
Cds2f/f;AlbCre
Cds2f/f;AlbCre+AAV-Cds2
B
sacrifice
0
1w
2w
3w
4w
Cds2f/f
AAV-TBG-Con
AAV-TBG-Mboat7
Cds2f/f;AlbCre
AAV-TBG-Con
AAV-TBG-Mboat7
C
Cholesterol (μg/mg liver weight)
***
*
Cds2f/f + AAV-Con
Cds2f/f + AAV-Mboat7
Cds2f/f;AlbCre + AAV-Con
Cds2f/f;AlbCre + AAV-Mboat7
D
TAG (μg/ mg liver weight)
**
*
Cds2f/f + AAV-Con
Cds2f/f + AAV-Mboat7
Cds2f/f;AlbCre + AAV-Con
Cds2f/f;AlbCre + AAV-Mboat7
E
AAV-TBG-Con
AAV-TBG-Mboat7
Cds2f/f
Enlarged
Cds2f/f;AlbCre
Enlarged
F
Primary hepatocytes
Ad-EGFP
Ad-MBOAT7-EGFP
Cds2f/f
Cds2f/f;AlbCre
LipidTOX
G
LD size (um)
****
****
Ad-EGFP
Ad-MBOAT7-EGFP
Ad-EGFP
Ad-MBOAT7-EGFP
Cds2f/f
Cds2f/f;AlbCre
H
LD
ER
Cyto
AAV-TBG-Con
AAV-TBG-Mboat7
DGAT2
Calnexin
ATGL
Tubulin
MBOAT7
55kDa
100kDa
55kDa
55kDa
55kDa
I
Pulse
Chase 5 h
Ad-EGFP+DMSO
Ad-MBOAT7-EGFP+DMSO
Ad-EGFP+ISO
Ad-MBOAT7-EGFP+ISO
FFA (nmol/mg protein)
Time (hrs)

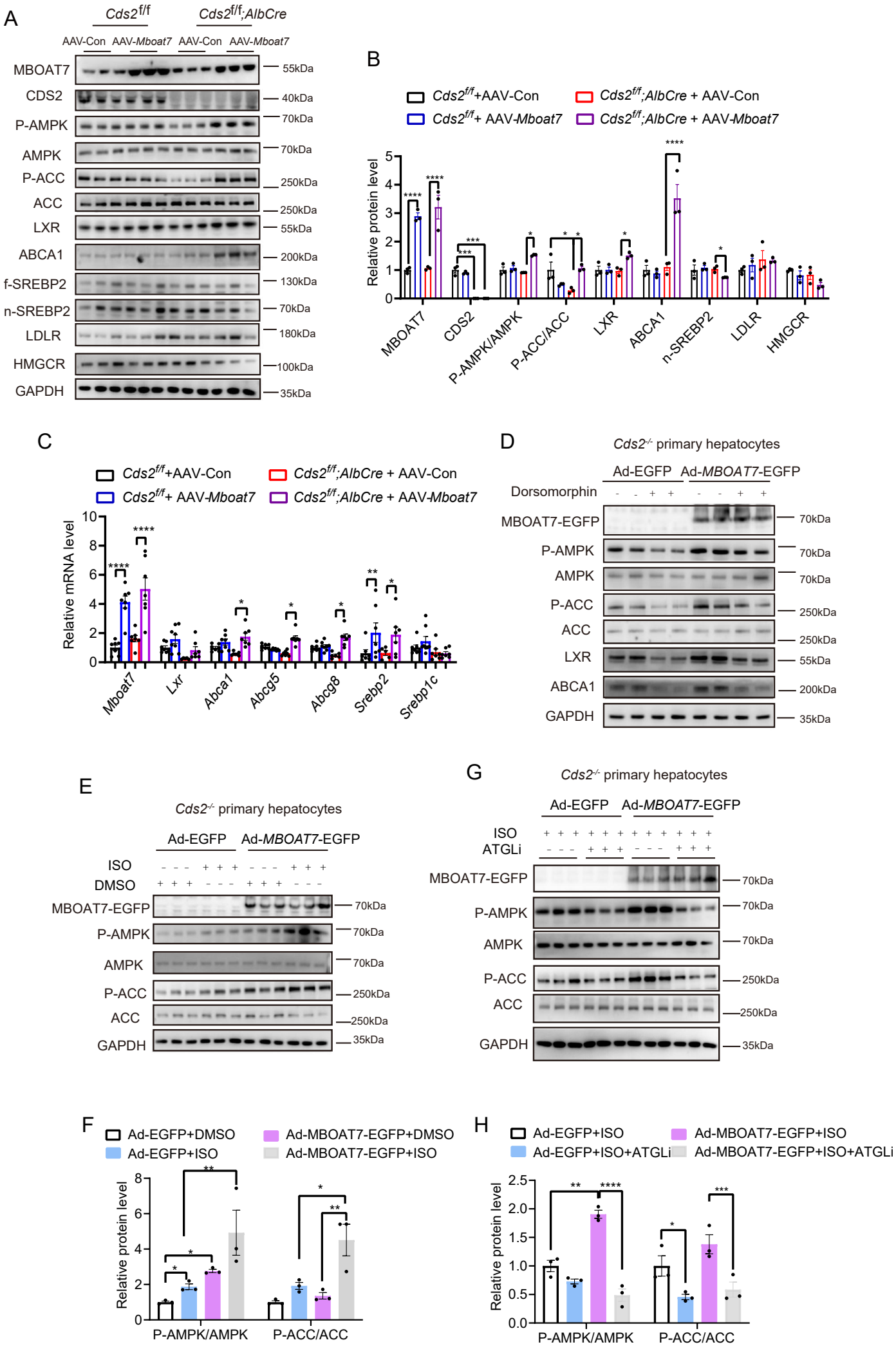
A
Cds2f/f
Cds2f/f;AlbCre
AAV-Con
AAV-Mboat7
AAV-Con
AAV-Mboat7
MBOAT7
CDS2
P-AMPK
AMPK
P-ACC
ACC
LXR
ABCA1
f-SREBP2
n-SREBP2
LDLR
HMGCR
GAPDH
55kDa
40kDa
70kDa
70kDa
250kDa
250kDa
55kDa
200kDa
130kDa
70kDa
180kDa
100kDa
35kDa
B
Cds2f/f+AAV-Con
Cds2f/f+ AAV-Mboat7
Cds2f/f;AlbCre + AAV-Con
Cds2f/f;AlbCre + AAV-Mboat7
Relative protein level
MBOAT7
CDS2
P-AMPK/AMPK
P-ACC/ACC
LXR
ABCA1
n-SREBP2
LDLR
HMGCR
C
Cds2f/f+AAV-Con
Cds2f/f+ AAV-Mboat7
Cds2f/f;AlbCre + AAV-Con
Cds2f/f;AlbCre + AAV-Mboat7
Relative mRNA level
Mboat7
Lxr
Abca1
Abcg5
Abcg8
Srebp2
Srebp1c
D
Cds2-/- primary hepatocytes
Ad-EGFP
Ad-MBOAT7-EGFP
Dorsomorphin
MBOAT7-EGFP
P-AMPK
AMPK
P-ACC
ACC
LXR
ABCA1
GAPDH
70kDa
70kDa
70kDa
250kDa
250kDa
55kDa
200kDa
35kDa
E
Cds2-/- primary hepatocytes
Ad-EGFP
Ad-MBOAT7-EGFP
ISO
DMSO
MBOAT7-EGFP
P-AMPK
AMPK
P-ACC
ACC
GAPDH
70kDa
70kDa
70kDa
250kDa
250kDa
35kDa
G
Cds2-/- primary hepatocytes
Ad-EGFP
Ad-MBOAT7-EGFP
ISO
ATGLi
MBOAT7-EGFP
P-AMPK
AMPK
P-ACC
ACC
GAPDH
70kDa
70kDa
70kDa
250kDa
250kDa
35kDa
F
Ad-EGFP+DMSO
Ad-EGFP+ISO
Ad-MBOAT7-EGFP+DMSO
Ad-MBOAT7-EGFP+ISO
Relative protein level
P-AMPK/AMPK
P-ACC/ACC
H
Ad-EGFP+ISO
Ad-EGFP+ISO+ATGLi
Ad-MBOAT7-EGFP+ISO
Ad-MBOAT7-EGFP+ISO+ATGLi
Relative protein level
P-AMPK/AMPK
P-ACC/ACC

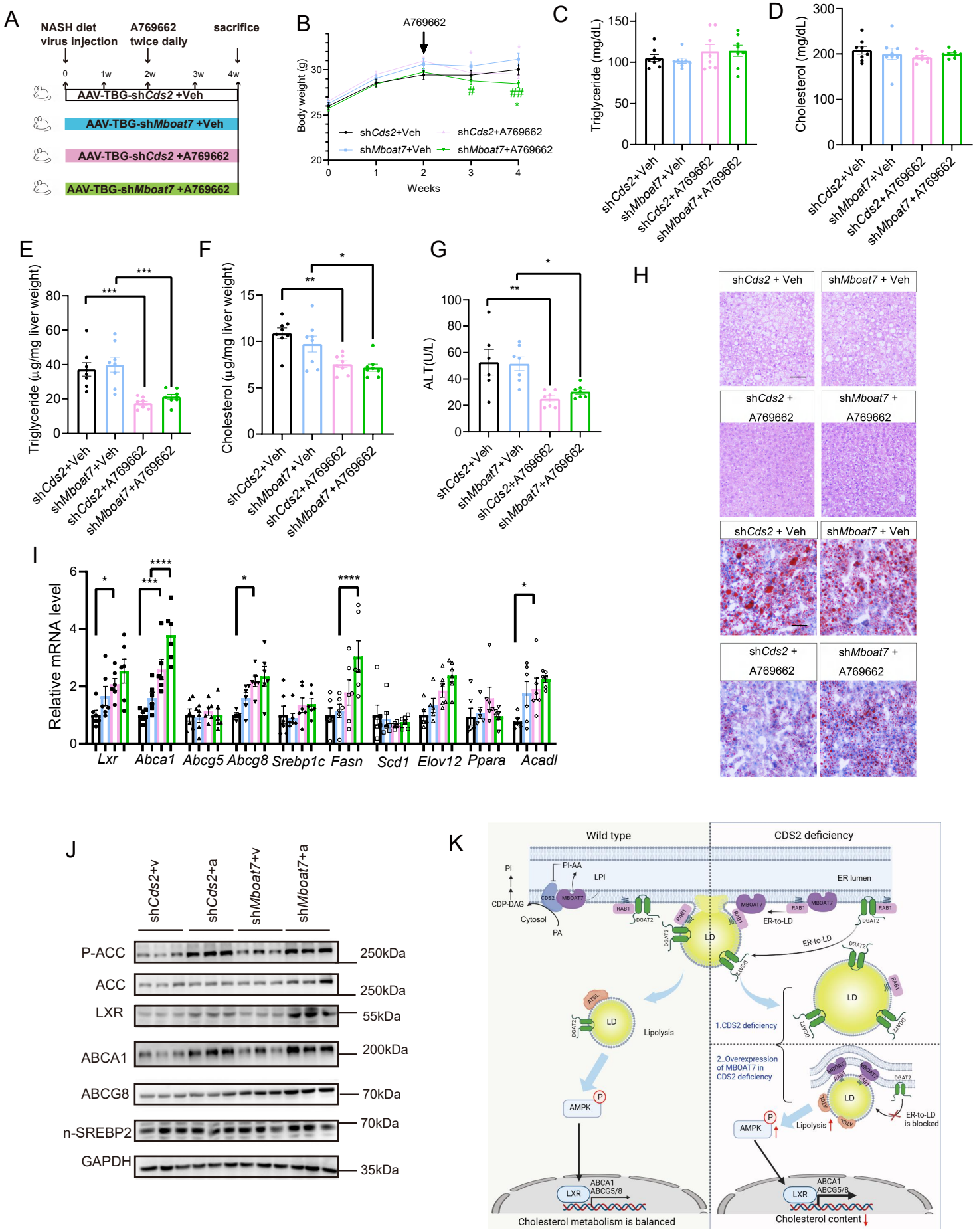
A
NASH diet virus injection
A769662 twice daily
sacrifice
0
1w
2w
3w
4w
AAV-TBG-shCds2 +Veh
AAV-TBG-shMboat7 +Veh
AAV-TBG-shCds2 +A769662
AAV-TBG-shMboat7 +A769662
B
A769662
Body weight (g)
Weeks
shCds2+Veh
shMboat7+Veh
shCds2+A769662
shMboat7+A769662
C
Triglyceride (mg/dL)
D
Cholesterol (mg/dL)
E
Triglyceride (μg/mg liver weight)
F
Cholesterol (μg/mg liver weight)
G
ALT(U/L)
H
shCds2 + Veh
shMboat7 + Veh
shCds2 + A769662
shMboat7 + A769662
I
Relative mRNA level
Lxr
Abca1
Abcg5
Abcg8
Srebp1c
Fasn
Scd1
Elov12
Ppara
Acadl
J
shCds2+v
shCds2+a
shMboat7+v
shMboat7+a
P-ACC
ACC
LXR
ABCA1
ABCG8
n-SREBP2
GAPDH
250kDa
250kDa
55kDa
200kDa
70kDa
70kDa
35kDa
K
Wild type
CDS2 deficiency
PI
PI-AA
LPI
CDP-DAG
Cytosol
PA
ER lumen
ER-to-LD
LD
Lipolysis
AMPK
1.CDS2 deficiency
2..Overexpression of MBOAT7 in CDS2 deficiency
ER-to-LD is blocked
LXR
ABCA1
ABCG5/8
Cholesterol metabolism is balanced
Cholesterol content